CHAPTER 3

Exploitation of Spatiotemporal Information and Geometric Optimization of Signal/Noise Performance Using Arrays of Carbon Black-Polymer Composite Vapor Detectors

ABSTRACT

We have investigated various aspects of the geometric and spatiotemporal response properties of an array of sorption-based vapor detectors. The detectors of specific interest are composites of insulating organic polymers filled with electrical conductors, wherein the detector film provides a reversible dc electrical resistance change upon the sorption of an analyte vapor. An analytical expression derived for the signal/noise performance as a function of detector volume implies that there is an optimum detector film volume which will produce the highest signal/noise ratio for a given carbon black-polymer composite when exposed to a fixed volume of sampled analyte. This prediction has been verified experimentally by exploring the response behavior of detectors having a variety of different geometric form factors. We also demonstrate that useful information can be obtained from the spatiotemporal response profile of an analyte moving at a controlled flow velocity across an array of chemically identical, but spatially nonequivalent, detectors. Finally, we demonstrate the use of these design principles, incorporated with an analysis of the changes in detector signals in response to variations in analyte flow rate, to obtain useful information on the composition of analytes and analyte mixtures.

I. INTRODUCTION

In most studies of vapor detector arrays to date, the detectors are placed in nominally spatially equivalent positions relative to the analyte flow path [1-3]. In such a configuration, any spatiotemporal differences between detectors are minimized, and the array response pattern is determined by the differing physicochemical responses of the various detectors towards the analyte of interest. The variations in analyte sorption amongst various detectors thus determines the resolving power of the detector array and determines the other performance parameters of such systems. In this work, we have deliberately placed detectors in spatially nonequivalent positions relative to the flow path of the sampled analyte. We demonstrate that the spatiotemporal response properties of such an array can be used advantageously to obtain information on the identity of analyte vapors and also to produce information on the composition of analyte mixtures.

Additionally, in most studies of detector arrays to date, the form factor of the individual detectors is constrained by factors related to the mode of signal transduction. For example, most film-coated QCM devices must have specified dimensions so that a resonant bulk acoustic wave can be maintained in the quartz crystal transducer element [4, 5]. Similarly, the geometry of SAW devices is constrained by the need to sustain a Rayleigh wave of the appropriate resonant frequency at the surface of the transducer crystal [4]. Each detector in a QCM or SAW array typically has an identical area and form factor; consequently, the array response is based solely on the different polymer/analyte sorption properties of the differing detector films. Although in principle these types of devices could be constructed with a range of form factors, relatively little attention has been focused on varying the form factors of the detector to optimize the signal/noise ratio (S/N) for a particular analyte. Recent work in our laboratories has focused on the use of chemically sensitive vapor detectors comprised of regions of electrical conductors interspersed amongst regions of insulating organic polymers [1].

The swelling of these films upon sorption of an analyte vapor produces a readily measured, dc electrical resistance change. Spray-coating deposition techniques using masked substrates permits the fabrication of such chemiresistor-type vapor detectors in virtually any geometry where the film can bridge two electrically conducting contact leads [6]. This freedom to explore various form factors allows convenient exploration of the geometrical aspects of sorption-based vapor detector design.

We demonstrate herein that different form factors of a given detector film in conjunction with specific types of analyte flow paths can provide very different detection performance for different types of analyte vapors. An analytical expression has been derived to predict the optimum volume of a detector film as a function of the sample volume and the analyte/polymer partition coefficient. Under certain conditions, detectors of very small areas are expected to have the best S/N performance, whereas for other conditions, relatively large detector areas are optimal. These predictions have been verified through measurements of the response properties of conducting polymer composite chemiresistor vapor detectors. We also demonstrate that, based on these principles, the use of an array of detectors that are nominally identical chemically, but which have different form factors relative to the analyte flow path, can provide useful information on the composition and identity of an analyte vapor. Finally, we report S/N data that allow comparisons between the detection limits of several polymer/analyte combinations using two different modes of signal transduction: frequency shifts in SAW devices and dc electrical resistance changes in composites of carbon black and insulating organic polymers.

II. THEORETICAL CONSIDERATIONS

A. Dependence of the Noise Power on the Area of a Carbon Black-Polymer Composite Vapor Detector

At open circuit, resistors exhibit voltage fluctuations whose power spectrum is constant as the frequency is varied. These fluctuations are known as Johnson noise. The root mean squared (rms) noise voltage density of this Johnson noise, V_{JN}, is related to the resistance, R, of a resistive detector as follows

$$V_{JN} = (4kTRB)^{1/2} \quad (1)$$

where k is Boltzmann's constant, T is the temperature in degrees K, and B is the bandwidth [7]. This Johnson noise is the fundamental lower limit on the noise of any device of resistance R, and its magnitude is independent of the volume or of other fabrication-dependent properties of the resistor. However, when current flows through most types of resistive materials, a voltage fluctuation is observed with a power spectral density that displays an inverse dependence on frequency. This additional noise, which is typically of the form $1/f^{\gamma}$ where $\gamma = 1 \pm 0.1$, is designated 1/f noise [8, 9].

Even for a series of resistors that are fabricated by an identical process, the magnitude of the 1/f noise depends on the volume, $\mathcal{V}$, of the resistor. When the correlation length of the resistive particle network is small compared to the physical length scale of interest, the 1/f noise of a resistance-based detector is expected to be proportional to $\mathcal{V}^{-1/2}$ [10]. For a given film thickness, this implies that the total noise of a resistive detector scales as $A^{-1/2}$, where A is the total area of the detector film between the electrical contact leads. This dependence requires that the magnitude of the 1/f noise, in the frequency window of the measurement, is much greater than the magnitude of the Johnson noise, so that the total noise is dominated by the 1/f contribution. As a consequence of Ohm's law, the power spectral density, $S_n(V)$, of the 1/f resistance noise

scales with the square of the bias voltage, V_b, applied to the resistor. The quantity of fundamental interest in characterizing the noise of a resistive detector element is thus

$$S_n = S_n(V_b)/ V_b^2 \quad (2)$$

where S_n is the relative noise power spectral density and V_b is the biasing voltage [10, 11]. In contrast to the Johnson noise, the level of the 1/f noise in carbon black-polymer composite resistors varies with many factors, including the structure of the carbon black, its volume fraction in the composite, the type of insulator, the resistivity of the composite, and the method of resistor preparation [10, 12].

B. Dependence of Signal/Noise on the Area of a Carbon Black Composite Chemiresistor

Given the above expectations for the scaling of the noise power of a chemically sensitive resistor with the volume of the detector film, we now consider how the signal produced by sorption of an analyte will depend on the volume of the detector film. Consider introducing a fixed quantity of an analyte into a sample chamber of total volume $\mathcal{V}_l$ to produce an initial analyte concentration C_v^i in the vapor phase (Scheme I). This analyte could either be introduced as a pulse of concentrated analyte into the volume $\mathcal{V}_l$ or by introducing a sampled volume of analyte in conjunction with a dead volume of carrier gas in the sampling path such that initially after the sampling process has been completed, an analyte concentration C_v^i is present in a total headspace volume $\mathcal{V}_l$. Assuming that no analyte is present initially in either the background gas or the polymer, the total number of moles of analyte available for sorption into the polymer is therefore $n_T = C_v^i \mathcal{V}_l$. Sorption of the analyte into a polymer of volume $\mathcal{V}_p$ will proceed with a polymer/gas partition coefficient, $K=C_p/C_v^{eq}$, where C_p is the concentration of analyte in the polymer phase, C_v^{eq} is the concentration of the analyte in the vapor phase, and both concentrations refer to the situation after equilibrium has been reached.

Assuming that the change in volume of the polymer phase due to analyte sorption, $\Delta\mathcal{V}_p$, is small compared to the value of the initial headspace volume $\mathcal{V}_l$ implies that $\mathcal{V}_l$

also equals the headspace volume after equilibrium has been reached (for typical detector film thicknesses of 0.2-1.0 μm, and for typical headspace thicknesses of greater than 0.1 cm, even 100% increases in film thickness due to sorption-induced film swelling will produce a negligible change in the headspace volume). Under these conditions, conservation of mass of analyte implies that

$$n_T = \mathcal{V}_l C_v^{\,i} = \mathcal{V}_p C_p + \mathcal{V}_l C_v^{\,eq} \qquad (3)$$

Hence,

$$n_T = \mathcal{V}_p C_p + \mathcal{V}_l C_p/K \qquad (4)$$

or

$$C_p = n_T/(\mathcal{V}_p + \mathcal{V}_l/K) \qquad (5)$$

We further assume that the signal, S, obtained due to sorption of analyte into the polymer is linearly related to the sorbed analyte concentration through a sensitivity factor, X_1, for each analyte/polymer combination [13]

$$S = X_1 C_p \qquad (6)$$

In the limit where the 1/f noise dominates the total noise of a chemically sensitive resistor, this measurement noise, N, scales as $\mathcal{V}^{-1/2}$ (vide supra). Hence one can write

$$N = X_2\, \mathcal{V}_p^{-1/2} \qquad (7)$$

where X_2 is a constant that is independent of the film volume.

The signal/noise is therefore

$$S/N = X_1 C_p/\, X_2\, \mathcal{V}_p^{-1/2} \qquad (8)$$

Substituting for C_p from Eq. (5) produces

$$S/N = (X_1/X_2)\, n_T[\mathcal{V}_p^{1/2} + (\mathcal{V}_l/K)\, \mathcal{V}_p^{-1/2}]^{-1} \qquad (9)$$

Multiplying both the numerator and denominator of the right hand side of Eq. (9) by $(K/\mathcal{V}_l)^{1/2}$ yields

$$S/N = (X_1/X_2)\, n_T\, (K/\, \mathcal{V}_l)^{1/2}\, [(\mathcal{V}_l/K)^{-1/2}\mathcal{V}_p^{1/2} + (\mathcal{V}_l/K)^{1/2}\, \mathcal{V}_p^{-1/2}]^{-1} \qquad (10)$$

With the substitution $\chi = \mathcal{V}_p K/\, \mathcal{V}_l$, Eq. (10) becomes

$$S/N = (X_1/X_2)\, n_T\, (K/\, \mathcal{V}_l)^{1/2}\, [\chi^{1/2} + \chi^{-1/2}]^{-1} \qquad (11)$$

This function is maximized when χ=1, i.e., when K $\mathcal{V}_p$/ $\mathcal{V}_l$=1, which implies that

$$\mathcal{V}_p = \mathcal{V}_l/K \qquad (12)$$

at maximal S/N ratio.

When $\mathcal{V}_p = \mathcal{V}_l/K$, Eqs. (3, 4) yield $C_v^{eq}\ \mathcal{V}_l=(1/2)\ n_T$ and $C_p\ \mathcal{V}_p=(1/2)\ n_T$. In other words, for a finite quantity of sampled analyte, the maximal S/N ratio is obtained when the detector volume equals the headspace volume $\mathcal{V}_l$ divided by the polymer/gas partition coefficient. This produces a situation in which equal numbers of moles of analyte are present in the polymer and vapor phases after equilibrium has been attained. In practice, the film thickness of the detector is typically as small as possible to minimize the time constant for sorbtion/desorbtion of analyte. Hence, at constant, minimized film thickness, Eqs. (9, 12) imply that there is an optimum detector film area for a given headspace volume and a given initial headspace analyte concentration. Smaller detector areas than this optimum value fail to exhibit optimally low noise, while larger detector areas result in the sorption of the fixed number of moles of analyte into too large of a polymer volume and therefore produce a reduced magnitude of signal after equilibrium has been reached. Another consequence of the analysis presented above is that the different response properties of a set of detectors having a common polymer sorbent layer, but having different form factors, can provide information on the value of K, if $\mathcal{V}_l$ is known and/or is held constant during the experiment. Below we evaluate the validity of these predictions for sorption-based detectors fabricated using carbon black loaded chemiresistors as exemplary systems.

III. EXPERIMENTAL

A. Materials

Poly (ethylene-co-vinyl acetate) with 25% acetate (PEVA), and poly(caprolactone) (PCL) were purchased from Scientific Polymer Products. The solvents n-hexane, n-decane, n-dodecane, n-tridecane, and n-hexadecane were purchased from Aldrich Chemical Corp, while toluene and methanol were purchased from EM Science. All solvents were used as received.

B. Fabrication of Substrates and Detector Films

1. Detector Film Fabrication

The carbon black-polymer composite suspensions used to form the detector films were prepared by dissolving 160 mg of polymer in toluene, followed by addition of 40 mg of carbon black (Cabot Black Pearls 2000) [1]. The mixtures were sonicated for 10 min and were then sprayed in several lateral passes using an airbrush (Iowata HP-BC) held at a distance of 10 to 14 cm from the substrate.

2. Substrates for Noise Measurements

For measurements of the noise properties of the detector films, glass microscope slides were coated with a 50 nm thick layer of Au on top of a 15-30 nm thick layer of Cr, in a pattern that produced rectangular gaps between two parallel metal contact regions. The ratio of the rectangular edge length to the gap length was 8:1, and this aspect ratio was held constant as the area of the gap was varied. After film deposition, this procedure resulted in detector films of similar resistance values that had systematically varying film volumes. Carbon black composite films containing either PEVA or PCL, and having areas of 0.080, 0.30, 1.2, 1.3, 5.0, 33.0, and 132 mm^2, with resistance values ranging from 70 to 160 kΩ, were then deposited onto these substrates. The resulting detector film thicknesses, which were between 180 and 300 nm for the PEVA films and between 60

and 120 nm for the PCL films, were measured with a Sloan Dektak model 3030 profilometer.

3. Substrates for Investigation of the Vapor Response of Chemically Equivalent, Spatially Nonequivalent Detectors

Two additional types of substrates were used for investigation of the spatiotemporal and geometric aspects of the chemiresistive vapor detectors. In the first set of experiments (Scheme II), a series of parallel Cr/Au contacts was formed on each side of 75 mm x 25 mm glass slides. These contact electrodes were 1.8 mm long and were separated by a gap of 0.4 mm. Each pair of electrodes, which defined the contacts for an individual detector, was spaced 5 mm apart, permitting formation of 15 individual detectors on each side of the glass slide. The area surrounding the electrodes was coated with a thin layer of Teflon.

Both sides of the substrate were masked, with the exception of a 5 mm by 75 mm rectangular region on each side of the substrate that was centered on the row of electrical contacts used to form the detectors. Through this mask, carbon black-PEVA composites were sprayed onto one side of the glass microscope slide and carbon black-PCL composites were sprayed onto the other side of the glass slide. After spraying, the carbon black-polymer films covered the entire length of these substrates (Scheme II). Two such substrates were prepared. On the first substrate, the resulting detectors had resistance values that ranged from 60 to 160 kΩ on the side sprayed with a PCL-carbon black composite and from 140 to 180 kΩ on the side sprayed with a PEVA-carbon black composite. The ranges on the second substrate were 70 to 110 kΩ on the side sprayed with the PCL-carbon black composite and 170 to 260 kΩ on the side sprayed with a PEVA-carbon black composite.

A low volume vapor sample chamber was custom fabricated for the vapor response experiments (Scheme II). The detector substrate was placed between two pieces of Al, each of which had a recess 3.5 mm wide and 400 μm in depth machined

along its length. Prior to assembly, a thin piece of Teflon tape was smoothed over the surface of the Al pieces and into the channel, effectively lining the top and the sides of the channel with an ≈ 60 μm thick layer of Teflon. This Teflon prevented contact between the analyte and the Al and also formed an airtight gasket between each Al piece and the substrate. Assembly of the Al pieces and the substrate created one shallow channel above the substrate and one shallow channel below the substrate, with each channel being 340 μm deep (400 μm channel depth minus 60 μm thickness of Teflon insulation) and 3.4 mm wide (3.5 mm machined width minus 2 x 0.06 mm thickness of Teflon insulation). Each channel spanned the entire length of the row of 15 detectors on its corresponding side of the substrate. The 3.4 mm width of the channel bounded the gas flow into a region that was less than the width of the detector film that had been sprayed onto the substrate. Hence, for the entire length of the channel, the detector film completely coated the substrate in the region adjacent to the channel.

4. Substrates for Investigation of the Vapor Response of Geometrically Optimized Detector Films

A second set of experiments (Scheme III) used rectangular 20 mm by 23 mm substrates that were fabricated by a commercial vendor (Power Circuits, Santa Ana, CA) using standard printed circuit board technology. Each of these substrates had electrical contacts deposited in a pattern that created a total of six detectors. Three detectors were located on the face of the substrate and three on the edge of the substrate. The three leading edge detectors were formed on the 840 μm thick edge of the substrate between parallel contacts that were located on each face of the circuit board. These detectors were located in positions 1e, 2e, and 3e on Scheme III. The 20 mm by 23 mm faces of the circuit board supported the three larger detectors, each of which had dimensions of 2.0 mm by 15 mm (positions 1f, 2f, and 3f in Scheme III). The electrodes that formed face detectors in the same location on the top and bottom of each substrate were wired together in parallel (i.e., the leads to detector 1f on the top face were connected in parallel

to the leads that addressed detector 1f on the bottom face of the substrate). On each substrate this arrangement therefore produced three face detectors, each having a total film area of 60 mm^2 (2 x 2.0 x 15 mm).

Six total substrates of this type were prepared. Three of these substrates were prepared by spraying PEVA-carbon black films onto the edge and face detectors of the substrates, and three by spraying PCL-carbon black films onto the edge and face detectors of the substrates. To prevent current leakage between adjacent detectors, the films of the all individual detectors were isolated from each other by masking during spraying to produce a narrow (1 mm wide) gap in the detector film between adjacent detectors. Each of the six substrates was sprayed from an independently prepared suspension of carbon black and polymer, but both faces and the leading edge of a given substrate were sprayed from the same suspension. The two faces of a substrate were coated with a film of approximately the same resistance, to create films of similar thickness on each side of a given substrate.

One substrate sprayed with a PEVA-carbon black composite and one sprayed with a PCL-carbon black composite were then assembled into a stack that also contained 760 μm thick Al plates and 105 μm thick Teflon spacers. This assembly created a set of small channels, each of dimensions 0.105 x 12 x 23 mm, that permitted vapor to be drawn over each set of face detectors. The Teflon spacers served as the side walls for each channel. The assembled stack was 4.59 mm high (2 x 0.840 mm + 3 x 0.760 mm + 6 x 0.105 mm). Three separate stack assemblies of this type were built.

The stack assemblies were fitted into an Al chamber that had an open front and a tube connector on the back (away from the leading edge detectors). This tube connector was piped to a vacuum pump through a combination airflow meter and regulator (Cole Parmer). Each of the three stack assemblies used in this experiment contained six total channels formed collectively between the two substrates, the three Al plates, and the two

walls of the chamber. Hence the volumetric flow of sampled gas through each individual channel was 1/6 of the volumetric flow of sample gas through the entire stack assembly.

C. Spectral Noise Measurements

A standard method was used to determine the noise of the detector films [10, 14]. Briefly, the films were placed into a metal box and were biased with a stack of batteries (18 volts total) that was connected in series to a 1 MΩ resistance. The 1 MΩ low-noise resistance was formed from ten 100 kΩ wire-wound resistors (Newark Electronics) that were soldered together in series. The bias voltage across the detector film was ac coupled to an SR560 wide-band low-noise voltage preamplifier (Stanford Research Systems), and the output of the preamplifier was sent to an SR785 dynamic signal analyzer (Stanford Research Systems) as depicted in Scheme IV. Using an average of 100 measurements, a power spectral density from 1 Hz to 800 Hz was collected for each film. Data collection occurred over a period of in excess of 100 s for each noise spectral power measurement. These spectra were divided by the square of the bias voltage applied to the chemiresistor, V_b^2, to yield the relative power spectral density S_n for each detector film [10].

A control experiment was performed to evaluate whether film-substrate contacts dominated the observed noise properties of the detectors. Two composite films of approximately the same thickness, film area, and resistance were fabricated, with one film deposited in five 0.38 mm gaps between ten parallel 5.0 mm wide Cr/Au electrical contact pads, and the other film deposited across only one 2.0 mm gap between two parallel 5.0 mm wide Cr/Au contact pads. The additional film/substrate contacts produced no change in the relative noise power of the films, suggesting that the measured noise resulted primarily from the properties of the bulk detector film as opposed to the properties of the film electrode contacts. The properties of commercial, low-noise, wire-wound resistors that had resistances similar to those of the carbon black composite films were also measured. The much lower noise values observed for these wire-wound

resistors, which are known to exhibit little or no 1/f noise, confirmed that the Johnson noise of the resistors plus any additional amplifier noise of the experimental setup was much lower than the 1/f noise observed for the carbon black composite films. No correction for the amplifier noise was therefore performed in analysis of the noise data of the carbon black composite detector films.

D. Vapor Flow Apparatus

An automated flow system was used to deliver pulses of a diluted stream of solvent vapor to the detectors [3]. The carrier gas was oil-free air obtained from the house compressed air source (1.10 ± 0.15 parts per thousand (ppth) of water vapor) controlled with a 28 L min^{-1} or a 625 ml min^{-1} mass flow controller (UNIT). To obtain the desired concentration of analyte in the gas phase, a stream of carrier gas controlled by a 625 ml min^{-1} or a 60 ml min^{-1} mass flow controller was passed though one of five bubblers. Saturation of the gas flow through the bubbler of interest was confirmed with a flame ionization detector (Model 300 HFID, California Analytical Instruments, Inc.). The saturated gas stream was then mixed with background air to produce the desired analyte concentration while maintaining the total airflow at the desired value for the linear flow chamber experiments (Scheme II) and at a constant value of 2 L min^{-1} for the geometrically optimized detector experiments (Scheme III).

For detectors in the linear flow chamber, the airflow was connected directly to the channel adjacent to the row of detectors. To produce the low flow rates required by this experiment, the analyte-containing vapor was generated at higher flow rates, and a constant 200 ml min^{-1} was subtracted with a flow-regulated pump, permitting the difference to flow into the detector chamber. This flow was then divided into the two equally sized openings of the two channels in the Scheme II chamber. The volumetric flow rates quoted below reflect the volumetric flow rate in each separate gap between the detector substrate and the Teflon-lined Al block.

For detectors arranged in the stack assembly of Scheme III, a constant output of 2 L min^{-1} from the vapor generator was directed at the front end of the sampling device through use of a Teflon tube that was slightly larger in diameter than the opening of the stack device. Vapor flow through the channels in the stack assembly was maintained at a volumetric flow rate of 75 ml min^{-1}, i.e., 12.5 ml min^{-1} per channel. The excess flow of 1.925 L min^{-1} flowed away from the stack device without proceeding through the channels or over the face sensors.

All exposed parts of the flow system were constructed from Teflon, stainless steel, or Al. The temperature during data collection was approximately 294 K, and the temperature was passively controlled by immersing the solvent bubblers into large tanks of water. For the linear row of detectors (Scheme II), vapor presentations were 300 s in duration, and analyte exposures were separated in time by at least 75 min to minimize any possible influence of the previous exposure. The analyte was delivered at a constant activity of $P/P^o = 0.10$, where P is the partial pressure and P^o is the vapor pressure of the analyte. For experiments with geometrically optimized detectors (Scheme III), the vapor presentations were 240 s in duration, separated in time by 25 min, and were conducted at a fixed analyte activity of $P/P^o = 0.050$. Flow experiments were performed separately on each of the three separate stack assemblies. Each stack assembly received 10 exposures to each of four analytes, and the order of these 40 total presentations was randomized with respect to the analyte identity and with respect to replicate exposures to a given analyte. A different randomized analyte presentation order was used for each of the three stack assemblies. A personal computer running programs developed with LabVIEW 5.0 controlled both the flow system and the data acquisition apparatus.

E. DC Resistance Measurements

DC resistance data were collected using a Keithley 2002 multimeter and a Keithley 7001 multiplexer. Shielded, twisted pair cables were used, and each resistance value was integrated over 2 or 10 power line cycles to reject 60 Hz pickup. Data were

processed using a program written in Microsoft Excel Basic. The relative differential resistance change, $\Delta R^{final}/R^{i}$, was calculated for each detector, where R^{i} is the initial resistance averaged over approximately 20 s prior to vapor presentation, and ΔR^{final} is the differential resistance change relative to R^{i}. The value of ΔR^{final} was evaluated over a period of approximately 20 s at a fixed time after initiating the vapor presentation. This time varied between the different types of experiments, either from 40 to 60 s, 200 to 220 s or 240 to 260 s after the start of the vapor presentation. No averaging was performed to collect the data represented in the figures which show the response characteristics of the detectors as a function of time. For ease of visualization on a common graph of the different absolute responses of the various detector/analyte combinations, the $\Delta R/R^{i}$ data in some figures have been normalized. In these figures, data were normalized by the mean response value, $(\Delta R/R^{i})_{j}$, of the detector in the physical position j for each set of identical exposures (i.e., for exposures to a common analyte, or for exposures to a common analyte at a common flow rate, as specified). The value for j was always chosen as the position of the detector to first physically encounter the analyte.

The rms noise, N_{rms}, of a detector was measured as the standard deviation of the data points obtained from the multimeter in the period immediately prior to each vapor presentation, divided by the average resistance value of the multimeter data points produced over that same measurement period. The period used to measure this baseline noise was equal to the time elapsed between determination of the baseline resistance and the determination of the differential resistance change upon analyte exposure. This ensured that the signals were measured in the same bandwidth as the noise. The multimeter was used to determine both the signal and noise values for this calculation because it was desirable to measure the signal and noise of the detectors using the same instrumental apparatus (i.e., the N in S/N is N_{rms}). The values of the S/N were calculated independently for each separate presentation of analyte to each detector. For the multimeter measurement of the noise of the films of different sizes described above, the

same analysis was used, except the noise was calculated over an interval of only 20 s, and 5 of these values, separated in time by 100 s, were averaged to generate N_{rms}. Unlike the values for S_n, which is a measure of the noise power, these noise values, N_{rms}, were first squared to yield N^2_{rms} prior to plotting them against film volume.

F. Determination of Polymer/Gas Partition Coefficients

Quartz crystal microbalance (QCM) measurements were performed on pure films of both PEVA and PCL at 294 K using 10 MHz resonant frequency quartz crystals and a measurement apparatus that has been described previously [15]. Twenty vapor presentations, each 120 s in duration and separated in time by 15 min, were performed at each of 4 concentrations (P/P^o = 0.010, 0.030, 0.050, 0.10) of n-hexane and of methanol. The order of vapor presentation was randomized with respect to analyte identity, analyte concentration, and repetition of conditions. The frequency shifts of the polymer-coated QCM crystals arising from deposition of the polymer film, $\Delta f_{polymer}$, were recorded as the difference in the resonant frequency of the crystal before and after deposition of the polymer film. The frequency change upon exposure to analyte vapor, $\Delta f_{analyte}$, was calculated as the difference in the resonant frequency of the film-coated crystal during exposure to the specific analyte vapor relative to the baseline resonant frequency of the film-coated crystal in background air. The baseline frequency was taken as the mean frequency value obtained for the film-coated crystal during a 30 s period immediately prior to exposure to the analyte, and the frequency during exposure to analyte vapor was taken to be the mean frequency value observed between 80 s and 110 s after the vapor exposure had been initiated.

IV. RESULTS

A. Noise Spectral Density Measurements for Carbon Black Composite Vapor Detectors

Fig. 1 displays the noise power spectral density, $S_n(V_b)$, between 1 Hz and 800 Hz for a set of carbon black composite thin film detectors as a function of the area covered by the composite between the electrical contact pads. The electrode contact dimensions in these experiments were scaled such that the resistance (≈100 kΩ) was approximately constant as the film area was varied. Any variation in the noise thus arose from the film area and not from a variation in response of the preamplifier to different absolute input resistance values. An additional advantage of maintaining a constant aspect ratio for the different volume films is to reduce the variation in the noise that has been observed in some thick-film resistors of different aspect ratios [16]. Fig. 1 also displays the power spectral density for a commercial, low-noise, wire-wound resistor.

The power spectral density of the carbon black-polymer thin film composites was well fit to a function of the form $S_n(V_b) \propto 1/f^{\gamma}$ with an exponent of γ=1.1. Some deviation from the 1/f behavior was observed at very low frequencies (< 5 Hz), but this deviation may have resulted from the mechanical contacts used to make connections to the Au/Cr/glass substrates. The noise power spectral density of the wire-wound resistor was much lower than the 1/f noise of any of the detector films at the frequencies investigated in this study.

Fig. 2 depicts the value of the $S_n * f$ product for carbon black composite detectors fabricated from PEVA or from PCL as a function of the volume of the detector film. For these comparisons, the data were taken as the value of S_n at 10 Hz to avoid the lower frequency contact noise. These values are directly comparable because they were taken at the same frequency, but the $S_n * f$ product was displayed because it is essentially independent of frequency for the 1/f region above about 5 Hz in frequency. Also shown

are the square of the noise values, N^2_{rms}, derived from analysis of the standard deviation of the baseline resistance values versus time as determined on these same films using the multimeter. The detector films used in these experiments were all approximately the same thickness, but the film volume data were calculated using the actual thickness values determined from profilometry measurements of the thickness of each detector film.

The N^2_{rms} and $S_n * f$ values decreased approximately linearly with the film volume, $\mathcal{V}$, with a plot of $S_n * f$ versus $\mathcal{V}$ for PEVA-containing carbon black composites having a slope of -0.95 (R^2= 0.989) and a plot of N^2_{rms} versus $\mathcal{V}$ having a slope of -0.91 (R^2= 0.964). For the PCL-containing carbon black composite films, the slope of $S_n * f$ versus $\mathcal{V}$ was -0.60 (R^2= 0.933), whereas the slope of N^2_{rms} versus $\mathcal{V}$ was -0.58 (R^2=0.833). It is difficult to perform a quantitative comparison between the $S_n * f$ and N^2_{rms} values, due to the impedance mismatch between the input amplifier of the multimeter and the resistive load of the detector, the variable bandwidth of the multimeter during various resistance readings, and other well-known electronic circuit considerations [17]. However, the inverse dependence of the N^2_{rms} value on the volume of the detector film is clearly seen in both sets of measurements. Deviations from a strictly linear dependence of the relative noise power on $\mathcal{V}$ with a slope of -1 have been observed previously for polymer film resistors, and have been explained by factors arising from the film-electrode contacts, inhomogeneities in film composition, and/or variability in film thickness over the measured detector area [12, 16]. The deviations that we observed may also have resulted from properties related to the relatively thin nature of the films used in this study.

B. Determination of Polymer/Gas Partition Coefficients

For a given volume of sampled analyte, the detector volume that will produce optimum signal/noise performance for a specific polymer/analyte combination can be calculated from Eq. (12) if the polymer/gas partition coefficient is known. Accordingly,

data for the partition coefficients of hexane and methanol into PCL and PEVA were determined using QCM measurements. Fig. 3a displays the QCM frequency shifts measured for PEVA films exposed to hexane or methanol, while Fig. 3b displays the frequency shifts measured for PCL films exposed to these same analytes.

The frequency shifts of the polymer-coated QCM crystals arising from deposition of the polymer film, $\Delta f_{polymer}$ and from sorption of the analyte vapor, $\Delta f_{analyte}$, were in total much less than 2% of the resonant frequency of the uncoated crystal. Under such conditions, prior work has concluded that mechanical losses are minimal and that the frequency shifts are predominantly due to changes in mass uptake [18], which can be calculated from the Sauerbrey equation [18, 19]. Polymer/gas partition coefficients were therefore calculated by fitting a line with a forced zero intercept through the $\Delta f_{analyte}$ versus concentration data for each polymer/analyte combination. The slopes of these lines were -4.36 ($R^2 = 0.9988$) and -0.910 ($R^2 = 0.9995$) for hexane and methanol, respectively, sorbing into PEVA, and were -0.612 ($R^2 = 0.9977$) and -0.930 ($R^2 = 0.9995$) for hexane and methanol, respectively, sorbing into PCL. The slopes of the resulting lines were converted into partition coefficients using

$$K = (10^6 \rho \mathcal{R} T m) / (M_w \Delta f_{polymer} P_{atm}) \qquad (13)$$

where $\mathcal{R}$ is the ideal gas constant (L atm mol^{-1} K^{-1}), ρ is the density (g ml^{-1}) of the polymer, T is the temperature (K), m is the slope of $\Delta f_{analyte}$ versus concentration (Hz/parts per thousand in air), M_W is the molecular weight (g mol^{-1}) of the analyte, $\Delta f_{polymer}$ (Hz) is the frequency shift corresponding to deposition of the polymer, and P_{atm} is the atmospheric pressure (atm). The partition coefficients for each analyte/polymer combination are displayed in Table 1.

Partition coefficients for the lower vapor pressure analytes, dodecane and hexadecane, were difficult to measure because these very low vapor pressure analytes adsorbed to the walls of the chamber and required long times as well as high analyte volumes to reach true equilibrium conditions. Instead, the values for these analytes were

estimated by multiplying the measured polymer/gas partition coefficients for hexane by the ratio of the vapor pressures of dodecane and hexadecane relative to that of hexane [20]. This is a good approximation provided that the activity coefficients do not vary significantly for sorption of these three alkanes into the polymers of interest. As displayed in Table 1, the polymer/gas partition coefficients varied from measured values of 10^2 for hexane and methanol to values of over 10^7 estimated for the lowest vapor pressure analyte, hexadecane.

The wide difference in vapor pressures between the analytes of concern is expected to have a significant influence on the physical array design for optimization of the signal/noise ratio as given by Eq. (9). In a chamber of headspace thickness of 1.0×10^{-2} cm, with a detector film thickness of 1.0×10^{-4} cm, the optimum detector area for a 1.0 cm^3 volume of an analyte sample for which the analyte polymer/gas partition coefficient is 1.0×10^2 is 1.0 cm^2. In contrast, for the same sampled volume, headspace thickness, and detector film thickness, a detector area of only 1.0×10^{-5} cm^2 produces maximum S/N performance for an analyte having a polymer/gas partition coefficient of 1.0×10^7. The implications of this wide variation in polymer/gas partition coefficient for optimizing the signal/noise performance of sorption-based vapor detectors are explored in detail below.

C. Spatiotemporal Response Data from Linear Arrays of Carbon Black-Polymer Composite Chemiresistive Vapor Detectors

The responses of an array of carbon black-polymer composite vapor detectors were investigated as a function of position relative to the location of analyte flow injected into the detection chamber. The pattern of the contacts beneath the film of carbon black-polymer composite produced an array of chemiresistive detectors that were arranged in a linear geometry, parallel to the analyte flow path, and which were spaced at 5 mm intervals downstream from the location of flow injection (Scheme II). The headspace volume was defined by the 3.4 mm width, 340 μm depth, and 75 mm total length of this

channel over the detector film. The area of the carbon black-polymer composite film spanned the entire length of the substrate and was sufficiently wide to ensure that the entire region of the substrate in contact with this vapor channel was coated with the detector film (Scheme II). Hence, in many respects this experimental apparatus is analogous to probing the spatiotemporal distribution of analyte in the sorbent phase after injection of a sample onto a gas chromatography column or to ascertaining spectroscopically the position of analyte in a thin layer chromatography experiment as a function of time.

Fig. 4 displays data collected for the array exposed in this configuration at a fixed, low carrier gas flow rate of three analytes of differing vapor pressure (hexane, dodecane, and tridecane) to a series of PEVA-carbon black composites. The data are the relative differential resistance values measured in a 20 s period after 240 s of continuous exposure to the various analytes of interest. The analyte exposures used to produce these data were randomized with respect to analyte identity and with respect to the 5 replicate exposures of each analyte at the concentration of interest.

For high vapor pressure analytes, the detectors all produced nominally identical, time-independent, responses to the analyte in the final 20 s of this 260 s exposure period. For example, the standard deviation of the mean response to hexane at $P/P^o=0.10$ for the 15 nominally identical detectors was less than 5% of the mean $\Delta R/R^i$ response value for this detector/analyte combination. This degree of reproducibility is consistent with prior reports that have evaluated the reproducibility of the response of carbon black-polymer composite detectors [1].

In contrast, during 260 s exposures to low vapor pressure analytes such as tridecane, the $\Delta R/R^i$ values observed from the detectors to first encounter the vapor stream were much higher than $\Delta R/R^i$ values observed for detectors located at positions remote from the injection location. The position-related variation in $\Delta R/R^i$ in response to the low vapor pressure analytes was clearly much greater than the standard deviation of

the $\Delta R/R^i$ value observed for replicate exposures to any of the analytes investigated. The trend was systematic in that the detectors closest to the analyte injection position displayed the highest $\Delta R/R^i$ values, the response decreased monotonically with position from the location of analyte injection, and the magnitude of the effect increased as the vapor pressure of the analyte decreased. Furthermore, for the low vapor pressure analytes, the change in mean response versus detector position far exceeded the standard deviation of the mean responses observed for these same detectors when exposed, in the identical apparatus, to analytes having high vapor pressures.

To conclusively prove that the effect was associated with the geometry of the flow system relative to the position of the detectors in the chamber, and not with any physicochemical inequivalence in the detectors themselves, the position of analyte injection was changed such that the flow proceeded in the opposite direction through the chamber, with analyte first encountering detector number 15 and finally encountering detector number 1 in Scheme II. The same analytes were used and the order of presentation was again randomized with respect to solvent identity and with respect to the five replicate exposures to each analyte; however, the exposure order was the same as that used when the flow proceeded from low to high detector number. As shown in Fig. 4, the detectors again provided essentially equivalent responses when exposed to high vapor pressure analytes at a volumetric flow rate of 6 ml min^{-1}. For low vapor pressure analytes, the highest $\Delta R/R^i$ values were again observed from the detectors that first physically encountered the vapor stream.

The effect of sorption of low vapor pressure analytes into the composite vapor detectors arranged in the linear geometry of Scheme II was also evident in the time-dependent response of the different detectors in the array. Fig. 5 displays the $\Delta R/R^i$ values of the detectors at various times during the course of exposure to hexane or dodecane, respectively. These exposures were performed in the same, low flow rate vapor response, experiment described above in which the analyte first encountered

detector number 1 in Scheme II. No averaging time window was employed in this representation of the data so that the response at a variety of times could be displayed. As shown in Fig. 5, at this flow rate all of the detectors reached a steady state response within 20 s during exposure to hexane, but no detector reached a steady state response during the first 240 s of exposure to the lower vapor pressure analyte, dodecane.

Position-related differences in the spatiotemporal response to different analytes are also apparent through examination of the temporal response of a single detector. Fig 6. shows resistance versus time data for exposure of a PEVA-carbon black composite to hexane (at $P/P^o = 0.10$) followed immediately by exposure to a mixture of hexane and dodecane (each at $P/P^o = 0.10$). These data were obtained at a relatively low carrier flow velocity (6 ml min^{-1}) on a PEVA-carbon black detector located at position 7 in Scheme II. Clearly as shown by Figs. 4-6, under these conditions, the different analytes can be distinguished based on their characteristic temporal responses on the detectors that arise from the interactions with the analyte flow in the detector chamber.

Fig. 7 displays similar data, collected on a different substrate, as a function of analyte flow velocity. Data presented are for two analytes, one having a high vapor pressure (hexane) and the other having a low vapor pressure (dodecane), both exposed to either PEVA-carbon black (Fig. 7a) or to PCL-carbon black (Fig. 7b) composite detector films. For each flow rate, hexane and dodecane were alternately presented to the detectors. This procedure was repeated for each of 5 flow rates, proceeding sequentially from the lowest volumetric flow rate to the highest volumetric flow rate. This 10 exposure protocol was then repeated in its entirety 4 times, producing 50 total exposures of analyte to the detectors. For high vapor pressure analytes (i.e., analytes with relatively small polymer/gas partition coefficients), all of the detectors exhibited essentially the same $\Delta R/R^i$ response values in the 20 s period after 240 s of analyte exposure at all tested flow rates, regardless of the position of the detector relative to the point of analyte injection. This is expected because the analyte sorption process determines the steady-

state value of $\Delta R/R^i$ [20], and because all of the detectors experienced essentially identical concentrations of analyte under such conditions.

Low vapor pressure analytes (i.e., analytes with large polymer/gas partition coefficients), however, produced different behavior. At high flow rates, all detectors produced essentially identical $\Delta R/R^i$ signals in the 20 s period after 240 s of analyte exposure, further confirming that the concentration of the analyte in proximity to each detector was similar and that the detectors themselves were very similar in response properties. However, at lower flow rates, lower $\Delta R/R^i$ values were observed in the 20 s period after 240 s of analyte exposure for the detectors to last encounter the vapor stream. To confirm that this effect was due to the physical location of the detector relative to the position of analyte flow injection, the direction of analyte flow in the chamber was again reversed and data were recollected for the entire sequence of analyte exposures. The lowest $\Delta R/R^i$ responses were again observed for detectors that were located farthest from the position of analyte injection. For both analyte injection positions, the responses of detectors located at positions remote from the position of analyte injection were still increasing at the end of the 260 s analyte exposure period.

At times shorter than the period required to produce time-independent responses on all of the detectors in the array, the concentration of the low vapor pressure analyte stream is clearly depleted by sorption into the first region of polymer composite film that it encounters, and the analyte concentration in the boundary layer that is exposed to the film is decreased further as the gas flow progresses along the length of the polymer composite. For analytes of low vapor pressure, all detectors produced essentially identical responses at high flow rates after 240 s of exposure time, whereas at sufficiently low flow rates different responses were still observed after this exposure time for detectors located in different positions relative to the position of analyte injection into the chamber. In this transitional region of behavior, analysis of the relative signal strengths of the detectors in the array can provide information on the partition coefficient of the

analyte into the polymer film of interest. Fig. 4 shows this effect quite clearly for hexane, dodecane, and tridecane.

D. Flow System Experiments with a S/N Enhancement Targeted Towards an Analyte's Vapor Pressure

The data presented above indicate that the noise decreases approximately as the square root of the detector area. Thus, for sufficient headspace volumes and quantities of sampled analyte so that the concentration of analyte sorbed into the polymer film remains constant as the detector area increases (as given by $K=C_p/C_v^{eq}$), an increased detector area will produce no change in the magnitude of the steady-state signal, a reduced value of the noise, and hence an increase in S/N ratio. However, for finite duration pulses of low vapor pressure compounds injected at low flow rates onto polymer films that have large polymer/gas partition coefficients, analyte sorption will only effectively occur onto the subset of detectors that are encountered initially by the analyte flow. In this situation, increasing the detector area decreases the S/N ratio and additionally masks the spatiotemporal dependence of analyte sorption that can be used to discriminate between analytes of differing polymer/gas partition coefficients (Figs. 4-7). In this section, we describe the results of experiments designed to exploit both aspects of these properties of detector/analyte/flow interactions. To investigate this trade-off between detector S/N and detector area, detector arrays arranged as depicted in Scheme III were exposed to various analytes of interest. In this configuration, a detector film was deposited onto the edge of a printed circuit board substrate, and two other detector films of nominally identical composition were then deposited onto the two faces of the substrate. The face detector serves in essence as one large collection of detectors arranged linearly as in Scheme II, thereby inherently averaging the responses, and providing reduced noise, for analytes with small polymer/gas partition coefficients. In contrast, the edge detector has a small area so that it can provide enhanced S/N performance for analytes with large polymer/gas partition coefficients. Two such substrates were oriented so that the analyte flow

encountered the leading edge of each detector first, and a component of this flow subsequently flowed along the faces of the substrate. One substrate had one polymer type forming its detectors and the other substrate had a separate, different carbon black-polymer composite material forming all of its detectors. The gaps between the substrates and the adjacent Al plates were sufficiently thin to insure that the flow would proceed in the desired direction. The entire experimental procedure and data collection were fully repeated 3 independent times, each time with 2 independently prepared substrates that were assembled into the configuration of Scheme III.

The reported $\Delta R/R^i$ responses, N_{rms} values, and S/N values (Table 1) for each stack assembly are averages over the three detectors of the same geometry (face or edge) on a single substrate for 10 exposures to a given analyte. In Table 1, the results of the experiments on the three independently prepared stack devices are displayed separately. The average responses to high vapor pressure analytes (hexane and methanol) on the face detectors were between 75 and 100% of the magnitude of the responses on the edge detectors, while the lowest vapor pressure analyte, hexadecane, produced responses on the face detector that were all less than 15% of the values observed on the edge detectors (Table 1). This difference was much greater than the standard deviation of the responses of either all of the face detectors or all of the edge detectors on given substrate to an exposure to the analyte of interest.

The detector films on the leading edge of the substrate had 1/24 the area of the films on the face of the detectors, and therefore exhibited higher noise levels than the detectors on the face of the substrate. Noise values, N_{rms}, in the dc resistance readings measured using the multimeter were on average eight times higher for the PCL edge detectors than for the PCL face detectors, and were on average four times higher for the PEVA edge detectors than the PEVA face detectors (Table 1). The high vapor pressure analytes produced similar $\Delta R/R^i$ values on both detector types when exposed to methanol or hexane, hence the face detectors exhibited S/N ratios that reflected the decrease in

noise produced by large volume detector films (Table 1). For 200 s exposures to hexane, S/N values were ≈ 6 times higher for PCL face detectors and were ≈ 4 times higher for PEVA face detectors than for the corresponding edge detectors. In contrast, for 200 s exposures to hexadecane, the analyte with the lowest vapor pressure, the S/N values were about twice as high on the leading edge detectors as on the face detectors. Clearly, the different geometric form factors and interactions with the analyte flow streamlines produced different performance characteristics from a S/N viewpoint for these different types of detectors.

The temporal evolution of the detector response properties can also be exploited to differentiate between analytes. As shown in Figs. 8a and 8b, the responses of the face and edge detectors to hexane were similar after 40 s of vapor presentation, and remained similar after 200 s. These hexane responses are similar in magnitude to the signals for dodecane after 200 s (Fig. 8b), and the two analytes could not easily be distinguished based on these data alone. However, the responses for these two analytes are clearly separable at 40 s (Fig. 8a), when the hexane has fully equilibrated with the given polymer film area but the dodecane is still being depleted from the analyte sample due to its very high polymer/gas partition coefficient. The separation of these analytes as a function of time therefore demonstrates an increase in the resolving power attainable through the use of such spatiotemporal response information in conjunction with a spatially ordered array of vapor detectors.

V. DISCUSSION

A. Detection Limits of Chemiresistor-Based Vapor Detectors

We have previously reported that the steady-state $\Delta R/R^i$ values for various carbon black-polymer composite chemiresistors are linearly dependent on analyte concentration over a range of analyte/detector combinations and analyte concentrations [21]. The noise measurements reported herein, in conjunction with the previously reported dependence of $\Delta R/R^i$ on the partial pressure of the analyte [20] and the analyte/polymer sensitivity factors that can be deduced from such plots, allow estimation of the detection limits for various analyte/carbon black composite detector combinations. Two limiting cases will be considered: a) high vapor pressure analytes, which have relatively small partition coefficients for sorption into the carbon black composite detectors, and b) low vapor pressure analytes, which generally sorb strongly and exhibit very large polymer/gas partition coefficients into the polymers of concern.

When the polymer/gas partition coefficient is relatively small, sufficient analyte will, in general, be present in the sampled volume to produce the equilibrium volume swelling of the entire available detector area. In this situation, too little detector volume is generally present to satisfy the optimum detector volume as given by Eq. (12). At constant film thickness, the steady-state $\Delta R/R^i$ value of a given carbon black-polymer composite is directly related to the swelling change of the film. Thus, a given analyte concentration should produce the same steady-state $\Delta R/R^i$ signal in the film regardless of the area of such a detector.

Under these conditions, the scaling of the S/N (in a given measurement bandwidth) with detector area is determined by the dependence of the noise on detector area. As discussed above, the background noise of the carbon black composite chemiresistors at low measurement frequencies scales as $A^{-1/2}$. The S/N, and thus the detection limits of a particular carbon black polymer composite detector towards a given

analyte, therefore scale as $A^{1/2}$. The use of a detector film having the largest practical volume possible (up to the limit of optimum volume indicated by Eq. (12), or the volume at which the 1/f noise, for the measurement bandwidth, falls below the Johnson noise and the total noise no longer exhibits a dependence on volume) is thus the optimum detector design under such conditions.

Table 2 reports the S/N values and deduced limits of detection for representative carbon black-polymer composite detectors with various vapor analytes, for 1 cm^2 of detector area. Table 2 also reports representative values taken from the literature for selected polymer-coated SAW vapor detectors [22]. For the given area, the detection limits are comparable for both types of signal transduction, although the carbon black composites exhibit somewhat higher sensitivity than the SAW devices for the analyte/polymer combinations chosen for comparison. We have only reported limits of detection as opposed to limits of classification; the former quantity depends only on the properties of the analyte/detector combination, while the latter quantity also depends on the test set of analytes presented to the array as well as on the algorithms used to perform the classification. In one particular situation evaluated in the literature, the limit of classification of an analyte was shown to be within a factor of three of the limit of detection of that same analyte, indicating that the limit of classification is likely to be on the same order of magnitude as the limit of detection, at least for some tasks [23].

In the limit where the analyte exhibits a very strong sorption into the polymer film of the carbon black composite detector, the S/N optimization methodology is quite different. As given by Eq. (5), the sorption process under such conditions will be limited by the amount of analyte in the sampled volume. The $\Delta R/R^i$ signal of the detector is proportional to the swelling change of the detector film [15], so increasing the detector area will reduce the signal (by diluting the fixed amount of sorbed analyte into a correspondingly larger volume of polymer). As long as the swelling is linearly dependent on the concentration of analyte sorbed into the polymer [15], this dilution will

produce a linear decrease in the $\Delta R/R^i$ signal with increased detector volume. Because the noise scales as $A^{-1/2}$ (at constant film thickness), the S/N under such conditions scales as $A^{-1/2}$ and small detector areas are favored. In fact, the design goal under such conditions is to insure that the most analyte is sorbed into the least area of detector film, and signals should only be acquired from the limited, highly analyte-swollen, portion of the detector. For example, this design principle is appropriate for applications in which 2,4-dinitrotoluene, a vapor component above buried land mines [6, 24, 25], or other low vapor pressure analytes, are being detected. This principle is exemplified in the detector arrangement of Scheme III.

This relationship also has implications for sample chamber design of vapor detector arrays. For example, assume that the analyte headspace is comprised of a vertical column equal in area to the area of the detector film, and that the detector film thickness is 1.0×10^{-4} cm. For $K=1.0 \times 10^2$, the sorbed analyte would come to equilibrium in a closed system with the vapor phase analyte that is contained in a headspace thickness of 1.0×10^{-2}. Increasing the thickness of the headspace would simply provide more analyte than is needed to attain the optimal S/N ratio for the detector response and would require introduction of more sample into the headspace chamber. Alternatively, larger detector areas could be used advantageously to obtain improved S/N ratios from the increased number of analyte molecules available in a thicker (closed system) headspace chamber. In contrast, for $K=1.0 \times 10^7$, a 1.0×10^{-4} cm thick detector film would sorb essentially all of the analyte from a closed system having a 1000 cm thick headspace. A 2.6 cm^2 area of such a detector film could sorb essentially all of the analyte in a 3.0×10^{-2} cm thick headspace (c.f. Scheme II) that is supplied at a continuous volumetric flow rate of 10 $cm^3\ min^{-1}$ for a period of 260 min. For shorter analyte injection times (at constant analyte flow rate), smaller detector areas are optimal because otherwise the fixed amount of analyte is distributed into too large a detector area,

thereby diminishing the magnitude of the signal and deleteriously affecting the S/N ratio of the detector.

Given the relationships reported previously between the mass loading of analyte and the $\Delta R/R^i$ values for carbon black composite vapor detectors [15], in conjunction with the background noise levels reported herein, detection limits can be evaluated in the high sorption/low analyte vapor pressure regime. At a noise level of ≈10 ppm, and with a $\Delta R/R^i$=0.10 produced at a mass loading of 5.0 μg of analyte sorbed into 1 cm^2 of polymer [15], the computed 3σ detection limit of a PCL-carbon black composite is 1.5 ng cm^{-2}. This value can only be reached in practice if an efficient sampling and delivery system is available, such that the full amount of the sampled analyte can be delivered effectively to the 1cm^2 area of the detector film. Of note is that the detection limit scales inversely with the film area and linearly with the efficiency of delivering analyte to the sampled film area.

In the intermediate sorption/partition coefficient regime, an optimum detector volume clearly exists for which the S/N, and therefore the detection limit performance, of a particular analyte/polymer combination is maximized. This detector volume, and consequently the optimum film area, depends on only the analyte/polymer partition coefficient and the sampled analyte volume available for sorption into the detector, and is readily calculated from Eq. (12). The S/N can therefore be optimized for different vapor pressure analytes through control over the form factor of the detector film, as demonstrated herein both theoretically and experimentally.

B. Geometric Considerations of the Detector for Optimum S/N Performance with a Fixed Sample Volume

The dependence of optimum detector area on the analyte/polymer partition coefficient can also be used advantageously in the classification of analytes and analyte mixtures. In such a system, analytes with a high polymer/gas partition coefficient (generally analytes with low vapor pressures) would be sorbed into the smallest detector

area possible, producing the largest signal and therefore the largest S/N ratio for that particular analyte/polymer/sampler combination. Higher vapor pressure analytes are, in turn, detected with higher S/N performance at detectors having larger film areas. In fact, an array of contacts spaced exponentially along a polymer film could be used advantageously to gain information on the sorption coefficients of analytes into polymers, and therefore can provide additional classification information on analytes and analyte mixtures relative only to equilibrium $\Delta R/R^i$ values on a detector film having a single, fixed form factor for all analytes. A relatively simple demonstration of this principle was performed herein, in which two analytes were not readily distinguishable based on their responses on a single type of detector located on the edges of the substrates, but the analytes were clearly distinguishable when information on the relative response values of detectors located on the edge versus the face of the substrate was used in the data analysis. Additional information is available if the analyte flow rate is also varied over the detector array.

Variation in the geometric form factor of detectors also could potentially have practical advantages in the implementation of instruments based on arrays of vapor detectors. Although information similar to that produced by a collection of spatiotemporally arrayed detectors could in principle be obtained from an analysis of the time response of a collection of detectors that are equivalent both geometrically and with respect to the point of analyte injection, the spatiotemporal implementation discussed above has the advantage that analytes are detected on films that have nearly optimal S/N for the analyte of interest. In addition, electronically referencing the response of a face detector to that of an edge detector, for example, would allow nulling of the response to a high vapor pressure analyte and subsequent amplification of only those signals arising from low vapor pressure analytes. Finally, deliberate variation in the analyte flow rate could be used to encode the analyte signal at higher frequencies, and use of a lock-in

amplifier centered at this higher frequency (where the magnitude of the 1/f noise is lower than at dc) would enhance the S/N of these detectors.

Another feature of note is the possible relationship of this type of detector design to the biological olfactory system. Sobel and co-workers have recently reported differences in human perception of binary odorant mixtures that contained an odorant having a high vapor pressure and an odorant having a low vapor pressure [26]. The perceptual changes were shown to be produced by differences in flow rate between the two nostrils of the human subjects. Although the mixture contained fixed concentrations of each odorant, the subjects perceived the mixture to be enriched in the lower vapor pressure odorant when sampled through the higher flow rate nostril, and the same mixture was perceived to be enriched in the higher vapor pressure odorant when sampled through the lower flow rate nostril. The perceived responses changed when the flow rates in the nostrils were naturally interchanged due to normal physiological processes. The authors concluded that the spatiotemporally dependent responses of olfactory receptors is useful to humans in resolving certain odor mixtures and in obtaining additional information on the composition of odorants [26]. The relatively primitive system investigated herein demonstrates an analogous principle in a non-biological array of broadly cross-reactive vapor detectors, and thus a differential measurement of the response of two conducting polymer composite detector arrays, sampling the same analyte at different injected flow rates, might provide an interesting platform for evaluating the degree to which spatiotemporal response information can be used to obtain additional classification information in odor detection.

VI. CONCLUSIONS

The dependence of the relative power spectral density on the volume of carbon black-polymer composite vapor detectors was of the form $S_n \propto 1/\mathcal{V}^n$, with n=1 for PEVA-carbon black detectors and n=0.6 for PCL-carbon black detectors in the frequency range of 1-800 Hz. Analytes with moderate polymer/gas partition coefficients produce the same $\Delta R/R^i$ response values on detectors of constant film thickness but of different area, so under these conditions the S/N is optimized for detectors of very large area. In contrast, for finite quantities of injected sample, analytes with high polymer/gas partition coefficients produce much larger $\Delta R/R^i$ values on detectors of small area that are positioned to best sample the injected analyte flow. For such detector/analyte combinations, detectors of small area will exhibit significantly better vapor detection sensitivity. Manipulation of the geometric form factor of carbon black composite vapor detectors thus provides a facile method for optimizing the S/N performance for a particular detector/analyte combination of interest. An array of nominally identical polymer-carbon black detectors arranged linearly relative to the analyte flow path produces different spatiotemporal response patterns for analytes having different polymer/gas partition coefficients. Analytes with moderate polymer/gas partition coefficients produce the same signals on all detectors over a range of flow rates, whereas before steady-state is reached on all of the detectors, analytes with very large polymer/gas partition coefficients produce signals that are highly dependent on the analyte flow rate and the spatial position of the detector in the array. Such a configuration produces useful information on the composition of binary analyte mixtures and adds classification information to an array of compositionally different conducting polymer composite vapor detectors.

VII. ACKNOWLEDGMENTS

We acknowledge NASA, DOE, the NIH, and an Army MURI for their generous support of this work.

VIII. TABLES

Table 1: Responses, Noise, and S/N for two Types of Polymer-Carbon Black Composite Detectors in the Configuration of Scheme III.[a]

Analyte	Vapor Pressure of Pure Analyte		log Partition Coefficient (log k)[b]		Stack Assembly	$\Delta R/R^i$ x 100				N_{rms}				S/N			
			PCL	PEVA		PCL		PEVA		PCL		PEVA		PCL		PEVA	
	P^o (Torr)	PPM [c]				edge [d]	face	edge	face	edge	face	edge	face	edge	face	edge	face
hexane	$1.28*10^2$	$1.71*10^5$	1.65	2.23	A	1.4±0.2	1.07±0.03	3.3±0.1	3.5±0.6	$(1.5±0.7)*10^{-3}$	$(1.9±0.5)*10^{-4}$	$(5±1)*10^{-4}$	$(8±2)*10^{-5}$	13±7	60±14	73±20	460±2
					B	1.1±0.4	0.77±0.04	3.6±0.3	2.5±0.1	$(2±1)*10^{-3}$	$(3.2±0.8)*10^{-4}$	$(9±2)*10^{-4}$	$(1.3±0.3)*10^{-4}$	5±2	26±9	44±12	200±4
					C	1.3±0.2	1.17±0.08	2.8±0.3	2.4±0.1	$(1.2±0.6)*10^{-3}$	$(1.8±0.2)*10^{-4}$	$(4±2)*10^{-4}$	$(2.7±0.9)*10^{-4}$	23±23	100±60	77±25	100±3
					mean	1.3	1.0	3.2	2.8	$2*10^{-3}$	$2.3*10^{-4}$	$6*10^{-4}$	$1.6*10^{-4}$	14	64	65	260
methanol	$1.02*10^2$	$1.36*10^5$	2.26	1.98	A	2.4±0.2	2.7±0.1	2.0±0.4	2.1±0.5	$(1.4±0.8)*10^{-3}$	$(2.0±0.5)*10^{-4}$	$(5±1)*10^{-4}$	$(9±2)*10^{-5}$	23±12	140±42	42±10	270±1
					B	3.3±0.5	2.4±0.2	1.8±0.3	1.61±0.08	$(3±1)*10^{-3}$	$(3.0±0.6)*10^{-4}$	$(9±2)*10^{-4}$	$(1.5±0.3)*10^{-4}$	14±5	80±16	21±5	120±2
					C	2.6±0.8	2.8±0.2	1.1±0.2	1.2±0.1	$(1.2±0.8)*10^{-3}$	$(1.3±0.7)*10^{-4}$	$(4±2)*10^{-4}$	$(2.6±0.9)*10^{-4}$	33±22	260±110	28±11	50±1
					mean	2.8	2.6	1.6	1.6	$2*10^{-3}$	$2.1*10^{-4}$	$6*10^{-4}$	$1.6*10^{-4}$	23	160	30	140
dodecane	$9.71*10^{-2}$	$1.29*10^2$	4.77[e]	5.35[e]	A	1.6±0.2	1.16±0.03	3.7±0.1	3.6±0.6	$(1.3±0.6)*10^{-3}$	$(2.0±0.4)*10^{-4}$	$(5±1)*10^{-4}$	$(9±0.3)*10^{-5}$	15±7	60±13	76±21	440±1
					B	1.2±0.4	0.88±0.07	3.8±0.3	2.6±0.1	$(3±1)*10^{-3}$	$(3.2±0.9)*10^{-4}$	$(9±2)*10^{-4}$	$(1.4±0.2)*10^{-4}$	5±2	30±10	45±14	190±3
					C	1.6±0.2	1.25±0.04	3.4±0.1	1.3±0.2	$(1.2±0.8)*10^{-3}$	$(9±5)*10^{-5}$	$(4±2)*10^{-4}$	$(2.5±0.7)*10^{-4}$	32±32	150±64	100±41	54±2
					mean	1.5	1.1	3.6	2.5	$2*10^{-3}$	$2.1*10^{-4}$	$6*10^{-4}$	$1.6*10^{-4}$	17	81	73	230
hexa-decane	$9.11*10^{-4}$	1.21	6.70[e]	7.35[e]	A	0.3±0.2	0.01±0.09	0.26±0.09	0.01±0.01	$(1.4±0.9)*10^{-3}$	$(1.9±0.3)*10^{-4}$	$(5±1)*10^{-4}$	$(8±3)*10^{-5}$	3±2	1±1	6±2	2±2
					B	0.3±0.3	0.02±0.03	0.4±0.1	0.02±0.04	$(2±2)*10^{-3}$	$(3.1±0.9)*10^{-4}$	$(9±2)*10^{-4}$	$(1.4±0.3)*10^{-4}$	2±1	1±1	5±2	1±3
					C	0.3±0.2	0.03±0.03	0.3±0.1	0.04±0.07	$(1.1±0.7)*10^{-3}$	$(1.2±0.6)*10^{-4}$	$(4±2)*10^{-4}$	$(2.3±0.7)*10^{-4}$	5±4	4±4	8±3	2±3
					mean	0.3	0.02	0.3	0.03	$2*10^{-3}$	$2.1*10^{-4}$	$6*10^{-4}$	$1.5*10^{-4}$	3	2	6	2

a) Data were averages of 10 randomized presentations of the 4 analytes each at P/P^o =0.050, across 3 copies of each of the 2 detector types, with each value representing 30 vapor/polymer interactions. The experiment was repeated for 3 independently prepared stack assemblies (A,B,and C). The data represent responses after 200 s of exposure to analyte. b) Determined from quartz crystal microbalance measurements on unfilled polymers. c) Vapor pressure of analyte expressed in ppm of air at 294 K. d) Edge refers to the leading edge sensors and face refers to the face sensors depicted in Scheme III. The uncertainties are expressed as 95% confidence intervals. e) Values were estimated based on measurement of K for hexane and correction for the differences in vapor pressure between hexane and the alkane of interest assuming constant activity coefficients for the sorption of the alkanes into a given polymeric phase.

Table 2: Limits of Detection for Carbon Black Polymer Composite Detectors and Polymer Film SAW Detectors

		LOD (μg/L)			
	polymer	benzene	cyclohexanone	hexane	nonane
Carbon Black Composite[a]	PEVA	1.8x10	1.5	$4.0x10^{1}$	1.3
	PCL	$5.2x10^{2}$	$4.5x10^{1}$	$1.3x10^{3}$	$4.8x10^{1}$
SAW[b]	poly[bis(cyanoallyl)siloxane]	$4.0x10^{2}$	$1.5x10^{1}$	$5.3x10^{3}$	$5.7x10^{2}$
	poly(methylphenylsiloxane)	$3.0x10^{2}$	$1.4x10^{1}$	$1.5x10^{3}$	$1.1x10^{2}$
	poly(phenyl ether)	$2.2x10^{2}$	$1.3x10^{1}$	$9.9x10^{2}$	$7.9x10^{1}$
	poly(isobutylene)	$2.6x10^{2}$	$3.2x10^{1}$	$3.5x10^{2}$	$1.9x10^{1}$

[a] Carbon black composite limits of detection are calculated from the slopes of $\Delta R/R^{i}$ vs. P/P^{o} at 294 K in [21] using 3σ noise values for 1 cm^{2} of the same film type at average experimental film thickness values of 230 nm for PEVA and 80 nm for PCL. [b] SAW values are taken from [22] for 158-MHz SAW oscillators at 298 K.

IX. SCHEMES AND FIGURES

Scheme I. Equilibration between a finite volume of sampled analyte and a finite volume of a sorption-based vapor detector film. Before equilibration, the initial analyte at a concentration C_v^i is introduced into a total headspace volume $\mathcal{V}_1$. Equilibration of analyte between the vapor and polymer phases results in an equilibrium concentration of analyte in the polymer phase, C_p, and an equilibrium concentration of analyte in the vapor phase, C_v^{eq}, such that C_p/C_v^{eq} =K, where K is the polymer/gas partition coefficient. The headspace volume $\mathcal{V}_1$ is essentially constant before and after analyte sorption provided that the change in volume of the polymer phase due to analyte sorption, $\Delta\mathcal{V}_p$, is small compared to the initial headspace volume $\mathcal{V}_1$.

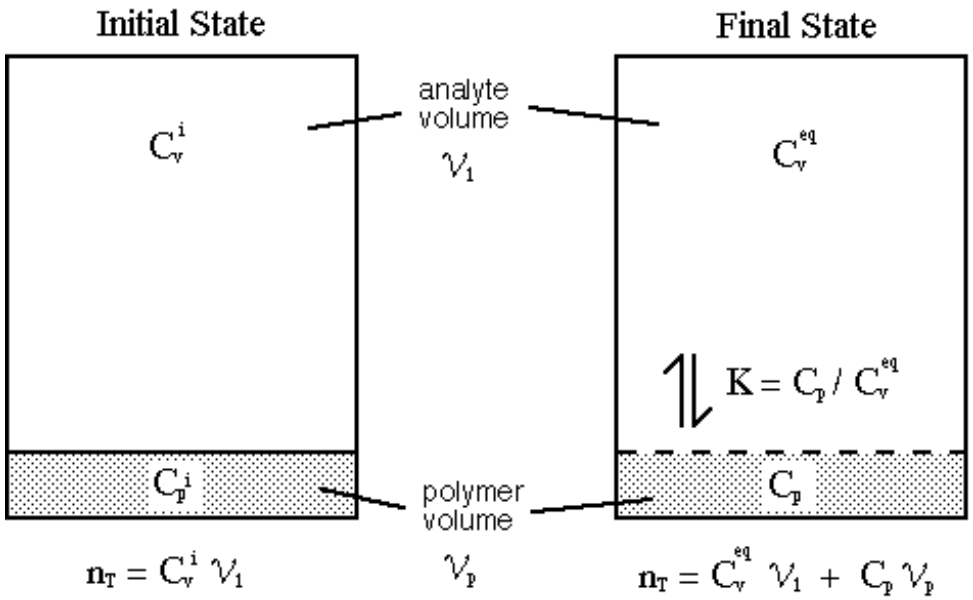

Scheme II. Layout of a substrate and associated sample chamber used to fabricate a linear array of detectors having a defined headspace and analyte flow configuration. a) A PCL-carbon black composite detector film was sprayed through a mask into a rectangular region of one side of the substrate, and a PEVA-carbon black composite film was sprayed into an identical pattern onto the other side of the substrate. Each polymer film coated a row of 15 pairs of Au/Cr contacts, creating 15 detectors on each side of the substrate. b) A two part Al chamber was then clamped onto both sides of the completed substrate, creating a Teflon-lined channel 340 μm deep and 3.4 mm wide that extended along each row of detectors for the entire length of both sides of the substrate. The wall of the channel that was adjacent to the substrate (i.e., the only wall that was not Al-coated Teflon) was fully spanned by the detector film. c) Airflow was then directed either from low to high detector position or from high to low detector position, as desired, by connecting the substrate/chamber assembly to the output of a vapor generator in conjunction with flow control equipment. Dimensioned drawings of the sample chamber are included in the appendix at the end of this chapter.

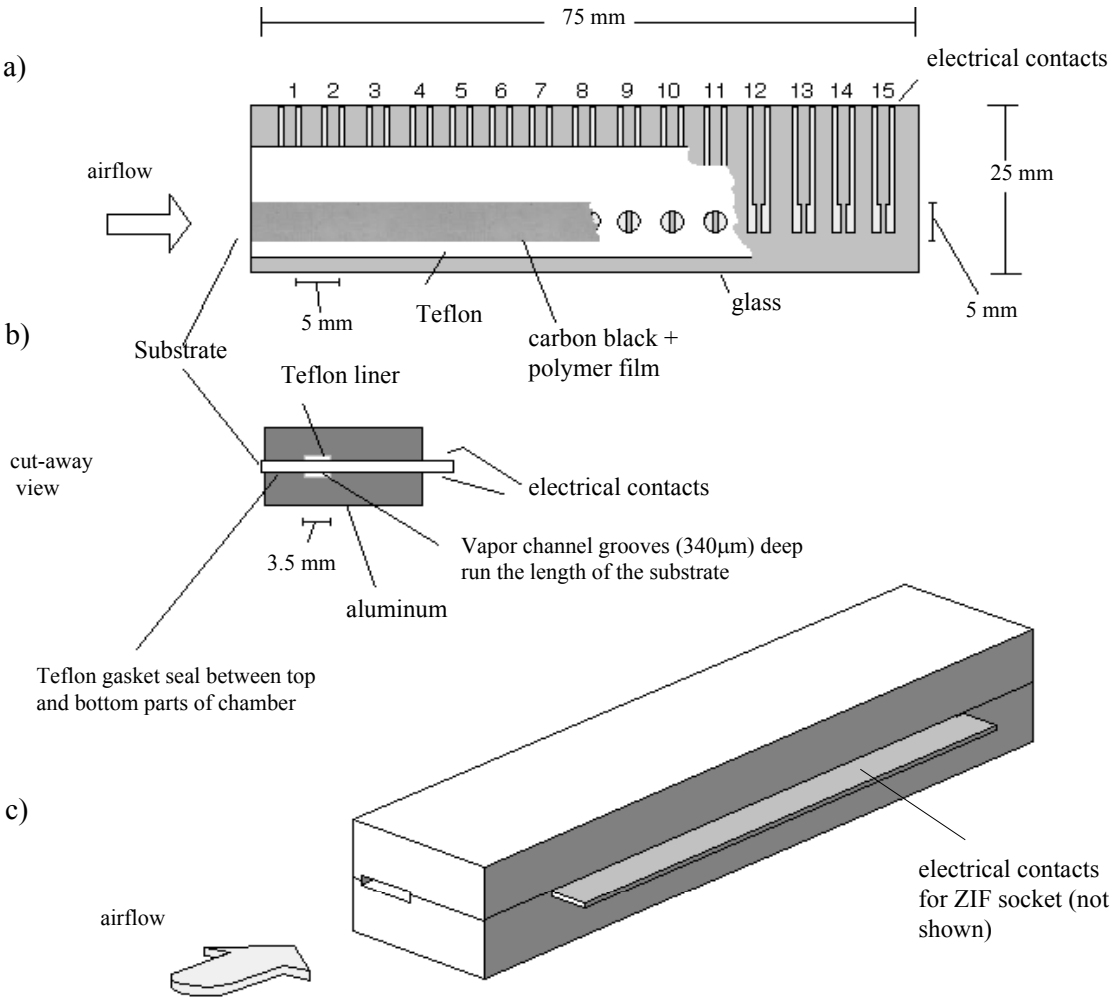
a)
75 mm
electrical contacts
1 2 3 4 5 6 7 8 9 10 11 12 13 14 15
airflow
25 mm
5 mm
Teflon
carbon black +
polymer film
glass
5 mm
b)
Substrate
Teflon liner
cut-away
view
electrical contacts
3.5 mm
Vapor channel grooves (340μm) deep
run the length of the substrate
aluminum
Teflon gasket seal between top
and bottom parts of chamber
c)
airflow
electrical contacts
for ZIF socket (not
shown)

Scheme III. Schematic of the printed circuit board substrates used to fabricate two types of detectors with different film areas. a) Each detector contained three detectors on the edge of the substrate (positions 1e, 2e, 3e in the Scheme) and three detectors on each face of the substrate (detectors on the face shown are in positions 1f, 2f, and 3f). Detectors in corresponding face positions on the two sides of a substrate were wired in parallel to form one bigger detector film. b) Two of these substrates were assembled into a stack structure constructed to direct the flow of an air stream containing an analyte vapor over first the small detectors on the edge of the substrate and subsequently over the larger detectors on the face of the substrate. The stack consisted Al plates alternating with detector-coated substrates, each interspaced with Teflon spacers. c) The stack was then inserted into an assembly that connected to a controlled flow from a vapor generator. Vapor flow through the assembly was controlled by connecting the output of the assembly to a regulated pump. The stack along with the Al walls of the assembly formed a total of six channels for vapor flow through the stack, first encountering the three detectors on the leading edge of each of the two substrates, then encountering the three two-sided detectors on the faces of each substrate. One substrate in an assembly was formed by spray deposition of a PEVA-carbon black composite detectors and the other substrate was formed by spray deposition of PCL-carbon black composite detectors.

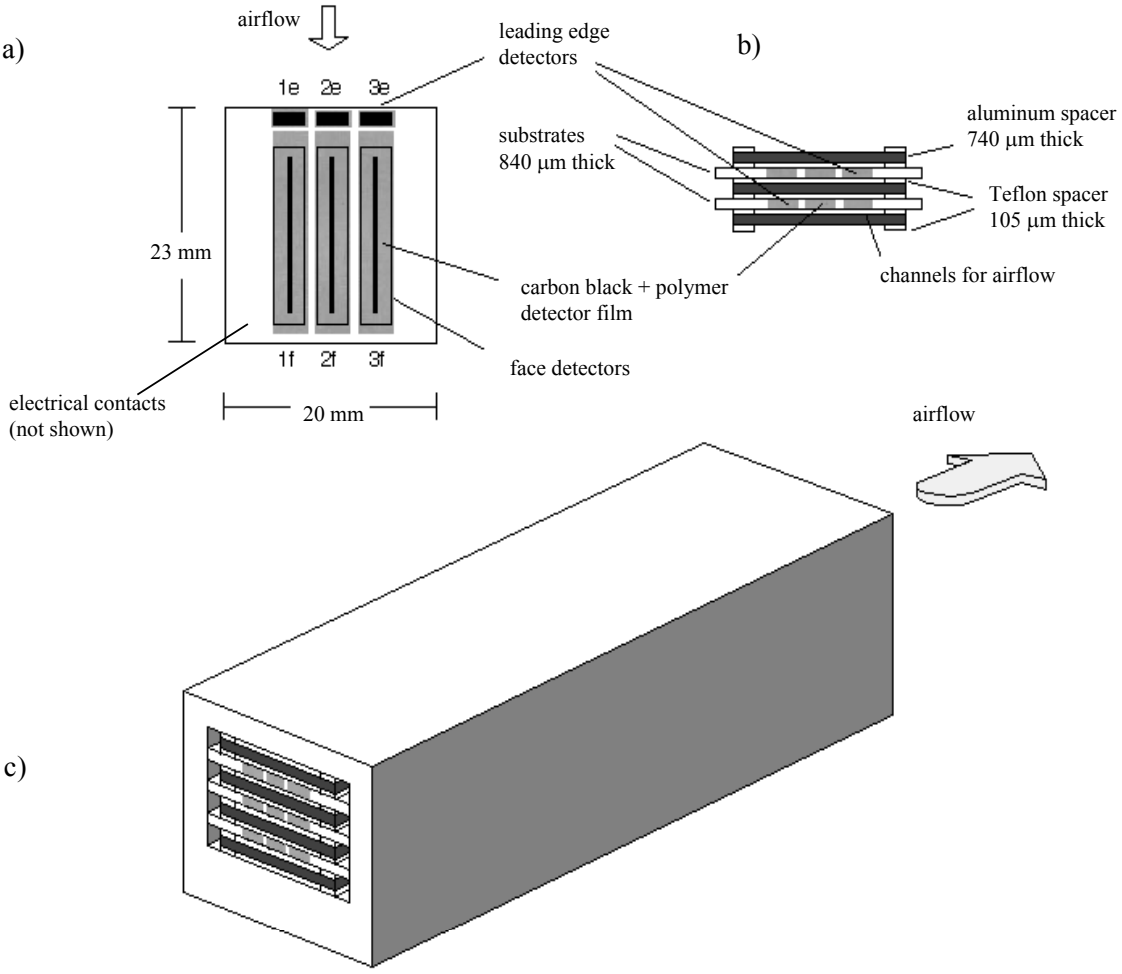
a)
airflow
leading edge
detectors
1e 2e 3e
23 mm
substrates
840 μm thick
carbon black + polymer
detector film
face detectors
1f 2f 3f
electrical contacts
(not shown)
20 mm
b)
aluminum spacer
740 μm thick
Teflon spacer
105 μm thick
channels for airflow
c)
airflow

Scheme IV. Schematic of the instruments and electrical connections used to measure the noise of carbon black-polymer composite detectors. a) A low-noise current source was constructed with a battery and a low-noise wirewound series resistance. The resulting voltage drop, V_b, across the sensor film was ac-coupled into a low-noise preamplifier, and the amplified signal was digitized and the noise power spectrum, $S_n(V_b)$, computed with a dynamic signal analyzer. b) A digital multimeter was also used to measure the resistance noise, N^2_{rms}.

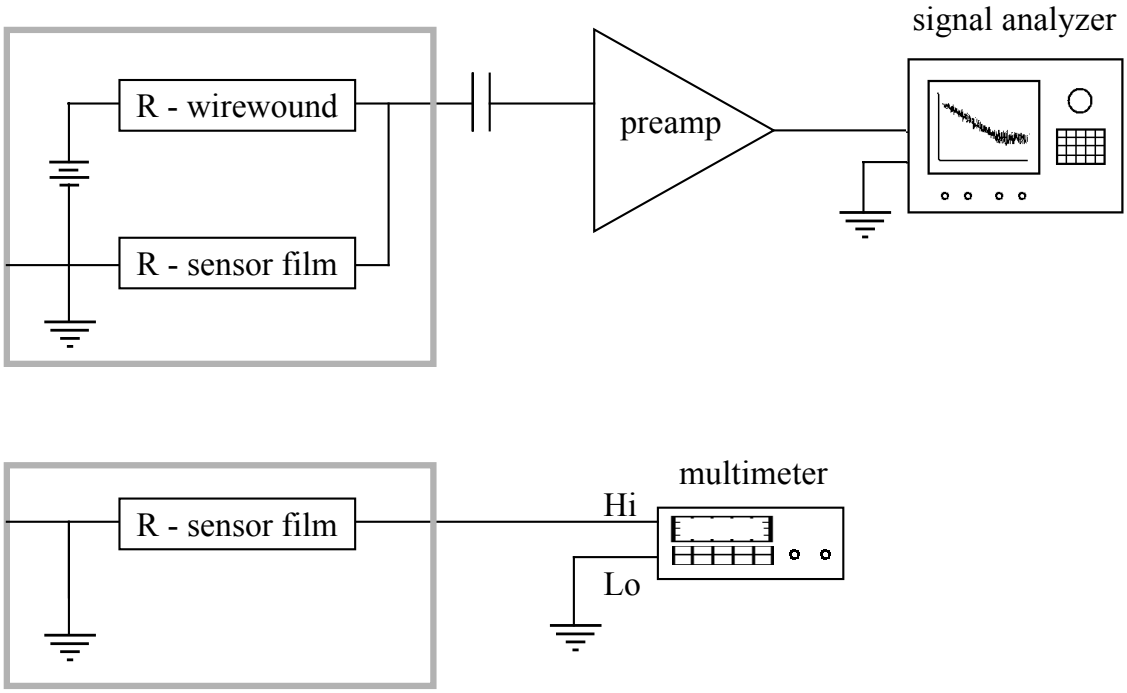

Fig. 1. Power spectral density of the noise, $S_n(V_b)$, versus frequency, f, for seven poly (ethylene-co-vinyl acetate), 25% acetate (PEVA)-carbon black composite detector films of varying area. The dimensions of the rectangularly shaped regions bridged by polymeric composite between the electrical contact pads were (in mm) 0.10 x 0.80, 0.20 x 1.60, 0.38 x 3.05, 0.40 x 3.20, 0.79 x 6.3, 2.03 x 16.3, 4.06 x 32.5. The PEVA-carbon black composite films were ≈ 230 nm in thickness as determined by profilometry. The dashed line indicates a fit of one such plot to a function of the form $S_n(V_b)=1\text{x}10^{-8}/f^{1.054}$. Also shown are data for a wire-wound, low-noise, 70 kΩ resistor.

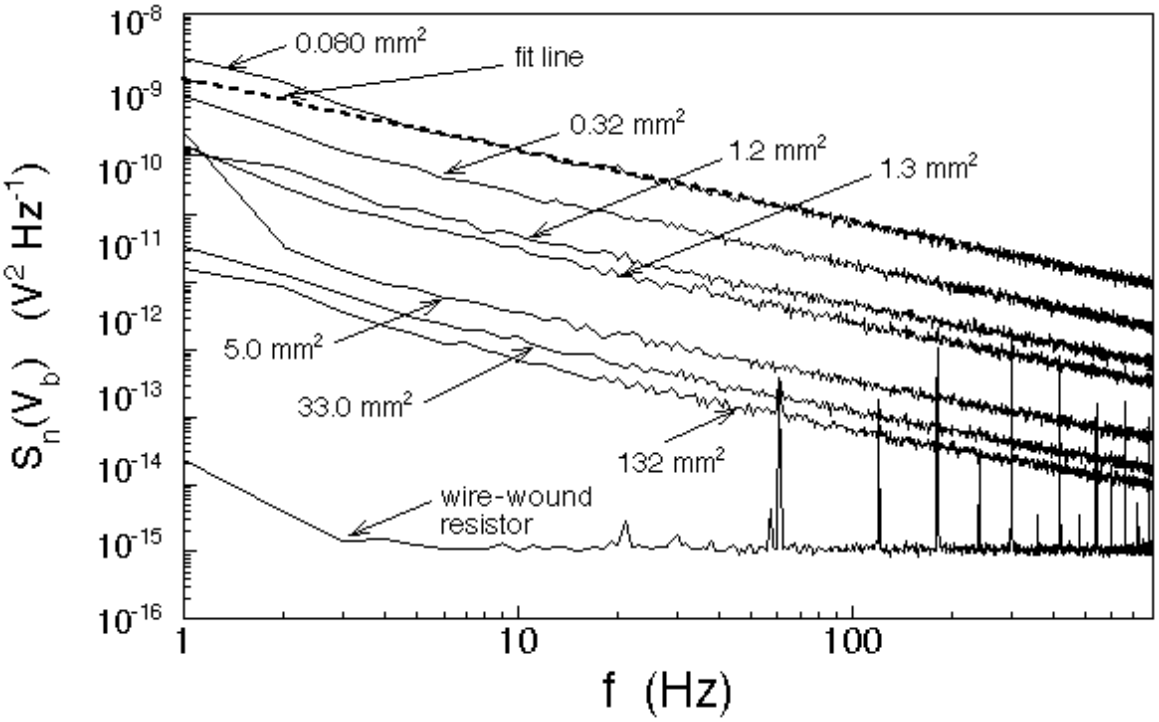

Fig. 2. Values of $S_n * f$ (open boxes) at 10 Hz and N^2_{rms} (filled circles) versus volume for carbon black composite detectors fabricated from a) PEVA and b) poly (caprolactone) (PCL). The PEVA-carbon black composite films were ≈ 230 nm in thickness and the PCL-carbon black composites were ≈ 80 nm in thickness as determined by profilometry.

a)

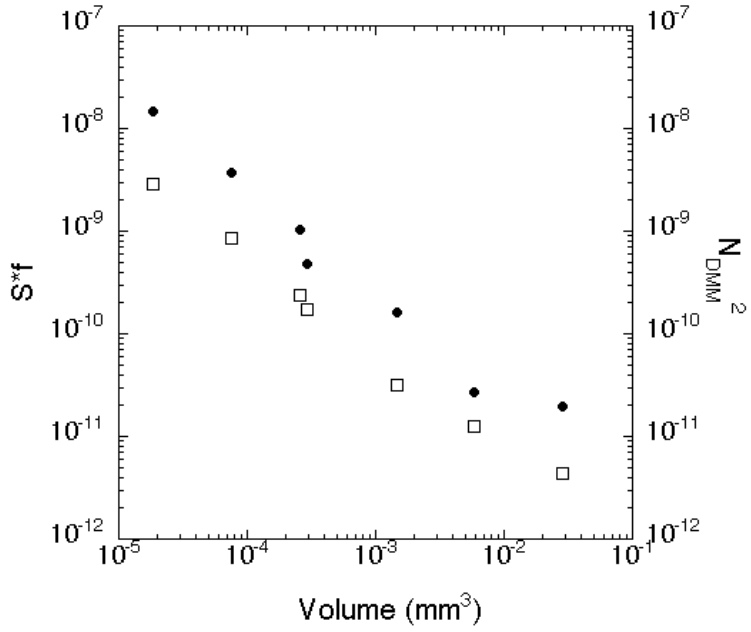

b)

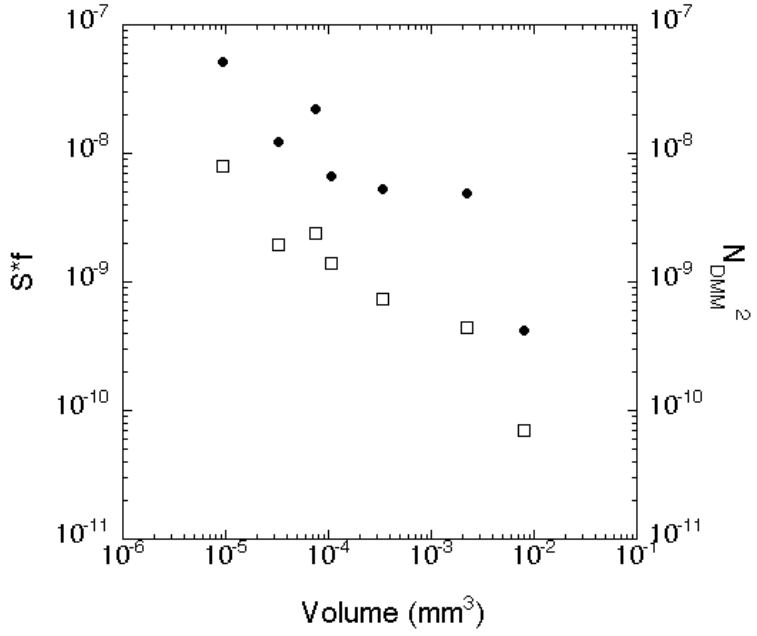

Fig. 3. Differential frequency changes, $-\Delta f_{analyte}$, of quartz crystal microbalances coated with a) PEVA and b) PCL polymer films (no carbon black) during exposure to hexane at P/P^o = 0.010, 0.030, 0.050, and 0.10 (1.7, 5.1, 8.5, 17 parts per thousand, ppth) and methanol at P/P^o = 0.010, 0.030, 0.050, and 0.10 (1.3, 4.1, 6.8, 14 ppth), where P is the partial pressure of analyte and P^o is the vapor pressure of the analyte at 294 K. Each data point represents an average of 20 $\Delta R/R^i$ responses, and the error bars indicate plus and minus one standard deviation around the mean. The frequency shifts corresponded to decreases in frequency upon exposure to analyte. Lines were fitted through these points with a forced zero intercept. The slopes of these lines were a) hexane: 4.36 (R^2 = 0.9988); methanol: 0.910 (R^2 = 0.9995); b) hexane: 0.612 (R^2 = 0.9977); methanol: 0.930 (R^2 = 0.9995). The frequency shifts due to coating the crystal with the polymer were -6835 Hz for PEVA and -4355 Hz for PCL.

a)

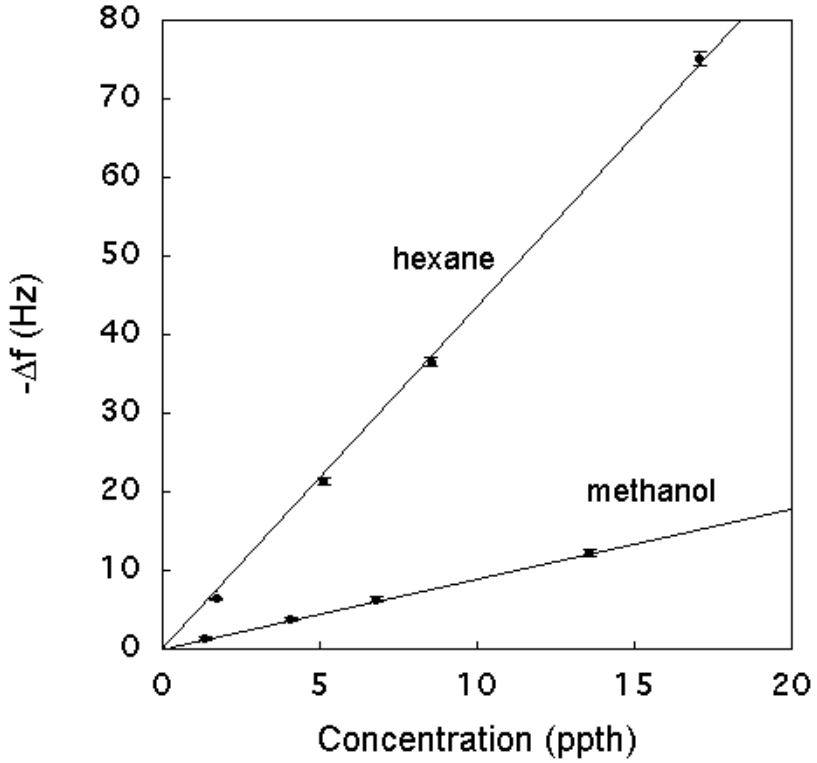
80
70
60
50
40
30
20
10
0
-Δf (Hz)
hexane
methanol
0
5
10
15
20
Concentration (ppth)

b)

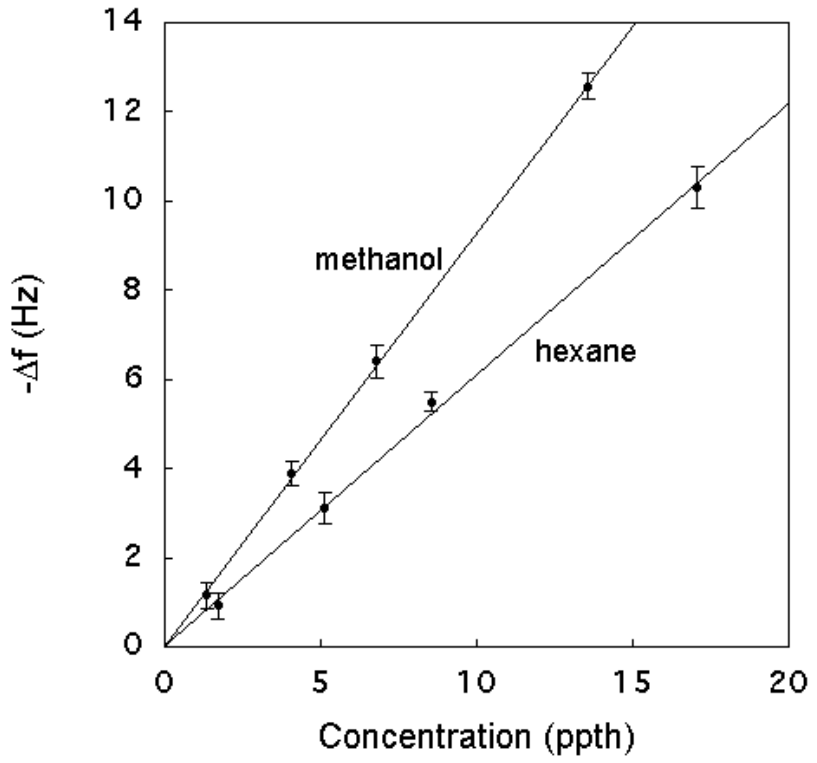
14
12
10
8
6
4
2
0
-Δf (Hz)
methanol
hexane
0
5
10
15
20
Concentration (ppth)

Fig. 4. Normalized relative differential resistance responses, $(\Delta R/R^i) / (\Delta R/R^i)_j$, of carbon black-PEVA composite vapor detectors exposed to three analytes: a high vapor pressure analyte (hexane), a moderately low vapor pressure analyte (dodecane), and a low vapor pressure analyte (tridecane, vapor pressure of 3.9×10^{-2} torr at 294 K), each at a constant activity of $P/P^o = 0.10$ and at a volumetric flow rate of 6 ml min^{-1}. Each point represents an average of 5 responses, and the error bars indicate plus and minus one standard deviation from the mean. Data were obtained from $\Delta R/R^i$ values observed between 240 and 260 s after initiation of exposure to the analyte of interest. The detectors were arranged in a linear geometry as depicted in Scheme II. For ease of visualization on a common graph of the different absolute responses of the various detector/analyte combinations, the data in this figure have been normalized relative to the mean response of the first detector that physically encountered the analyte. The solid lines indicate responses when the analyte flowed in the direction from the leftmost detector (corresponding to the detector with the lowest numbered position) to rightmost detector. These data (and associated standard deviations) were normalized to the mean response value of the detector in position 1 in the array (j=1) for the 5 exposures to the analyte of interest. The normalization constants (values by which the data were multiplied for display on the plot) are 10.8, 16.7, and 32.1, for hexane, dodecane, and tridecane, respectively. The dashed lines indicate responses recorded when the same row of detectors was exposed to vapor flowing in the opposite direction through the detector chamber; consequently, these data (and associated standard deviations) were normalized to the mean response value of the detector in position 15 in the array (j=15) to the 5 exposures of the analyte of interest. Normalization constants for these data are 10.4, 15.3, and 30.2, for hexane, dodecane, and tridecane, respectively. Analytes were delivered in a random order during an individual experiment, but the exposure order when analyte entered from the right was identical to the exposure order for experiments in which analyte entered the array from the left of the substrate as displayed in Scheme II.

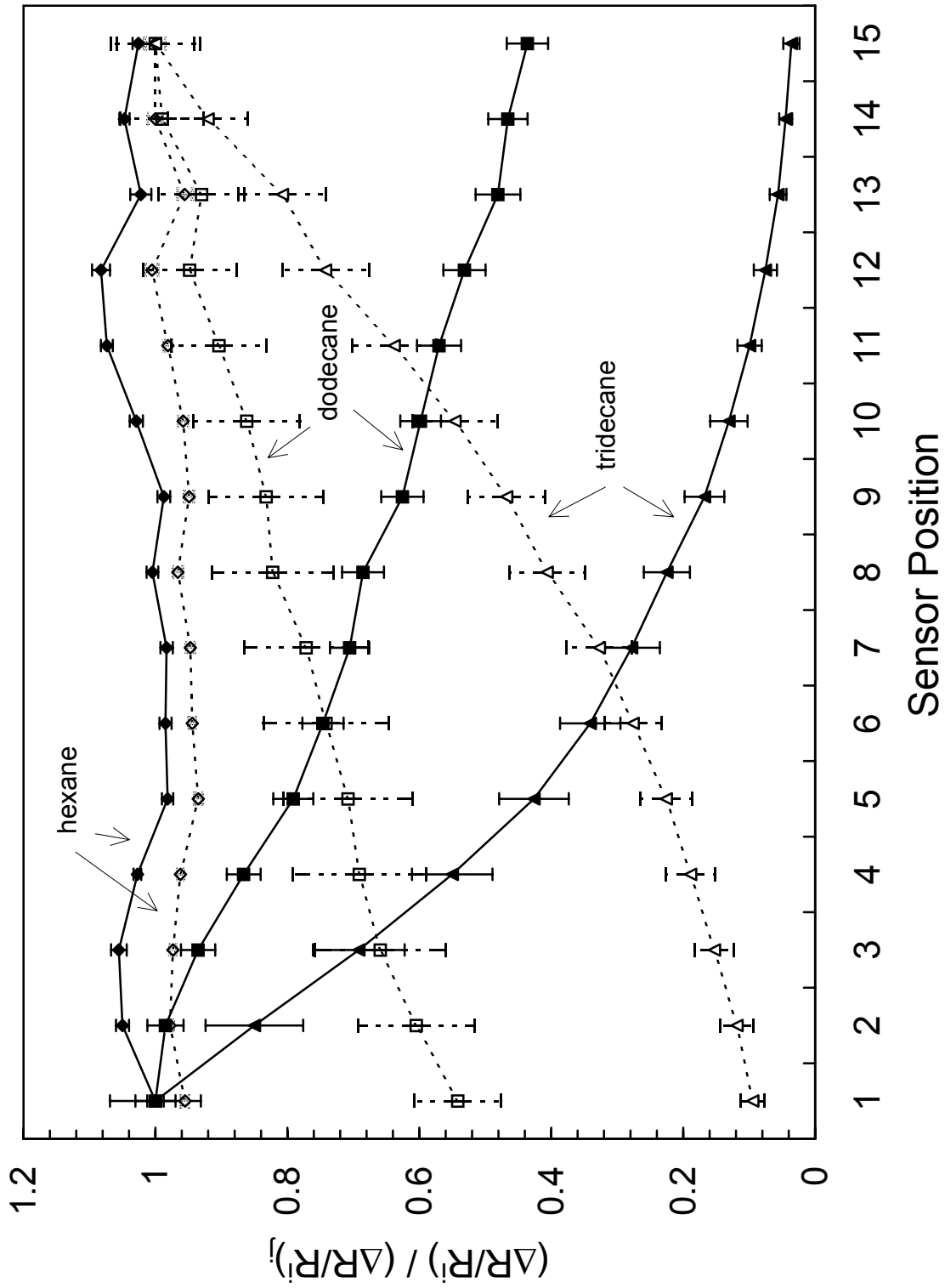
hexane
dodecane
tridecane
(ΔR/R)ⁱ / (ΔR/R)ⁱⱼ
Sensor Position
0
0.2
0.4
0.6
0.8
1
1.2
1
2
3
4
5
6
7
8
9
10
11
12
13
14
15

Fig. 5. Relative differential resistance responses, ($\Delta R/R^i$), of carbon black-PEVA composite vapor detectors configured as indicated in Scheme II for each detector position as a function of time during exposure to analyte vapor. These detectors were exposed to two analytes: a high vapor pressure analyte (hexane), indicated with a dashed line, and a moderately low vapor pressure analyte (dodecane), indicated with a solid line. Each analyte was delivered in random order at a constant activity of $P/P^o = 0.10$ and at a volumetric flow rate of 6 ml min^{-1}. The analyte flow entered first encountered detector 1 in Scheme II. Data for each analyte are displayed as $\Delta R/R^i$ values calculated at the specific times (20, 90, 180, 240 s) after initiation of the vapor exposure of interest. Each point represents an average of 5 values produced by independent exposures to the analyte of interest, and the error bars indicate plus and minus one standard deviation from the mean.

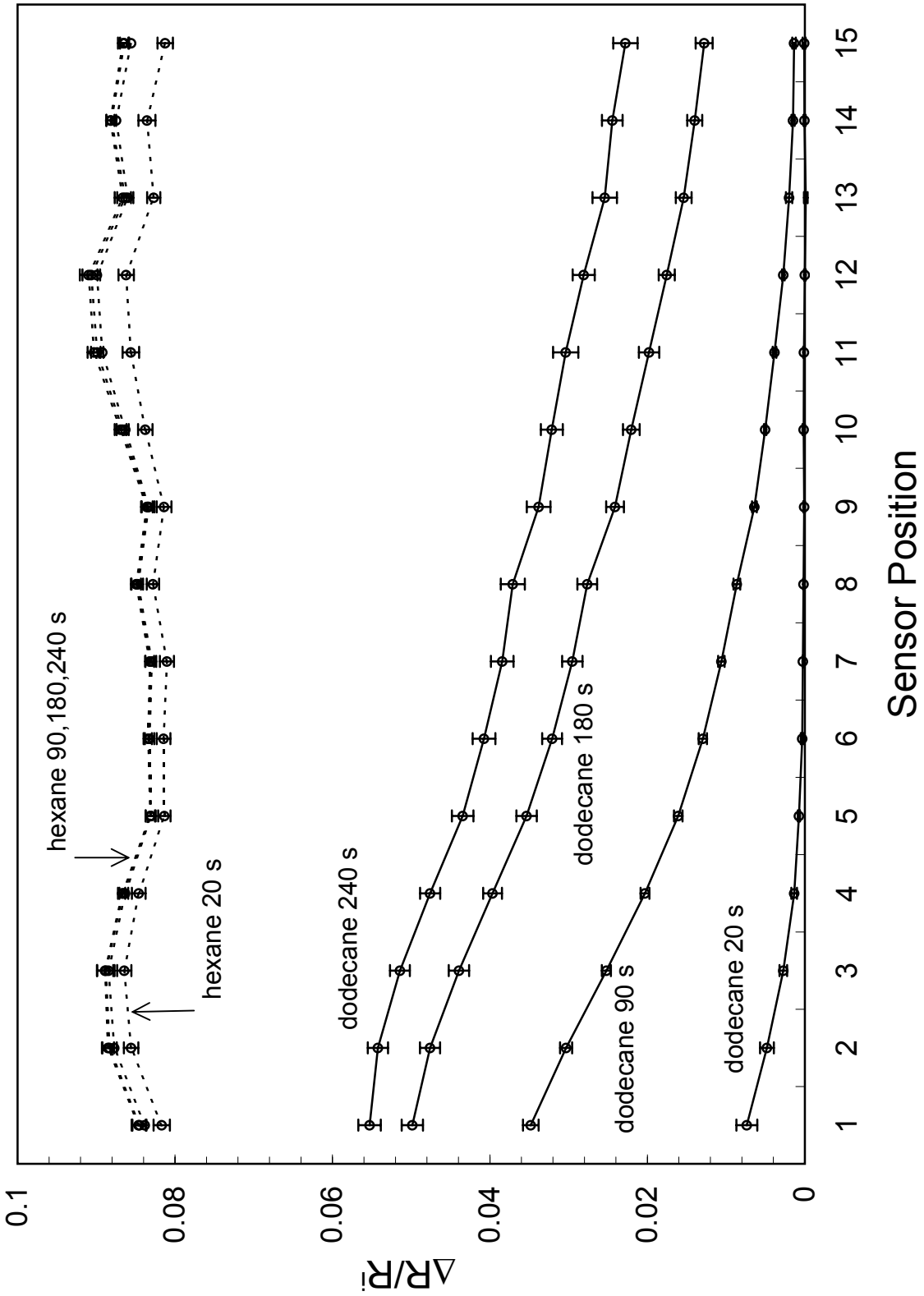
hexane 90,180,240 s
hexane 20 s
dodecane 240 s
dodecane 180 s
dodecane 90 s
dodecane 20 s
ΔR/R
Sensor Position
0
0.02
0.04
0.06
0.08
0.1
1
2
3
4
5
6
7
8
9
10
11
12
13
14
15

Fig. 6. Resistance response versus time for a PEVA-carbon black composite detector (located at position 7 in Scheme II) exposed to hexane at $P/P^o = 0.10$ from 300 to 600 s, and then to a mixture of both hexane at $P/P^o = 0.10$ and dodecane at $P/P^o = 0.10$ from 600 to 900 s.

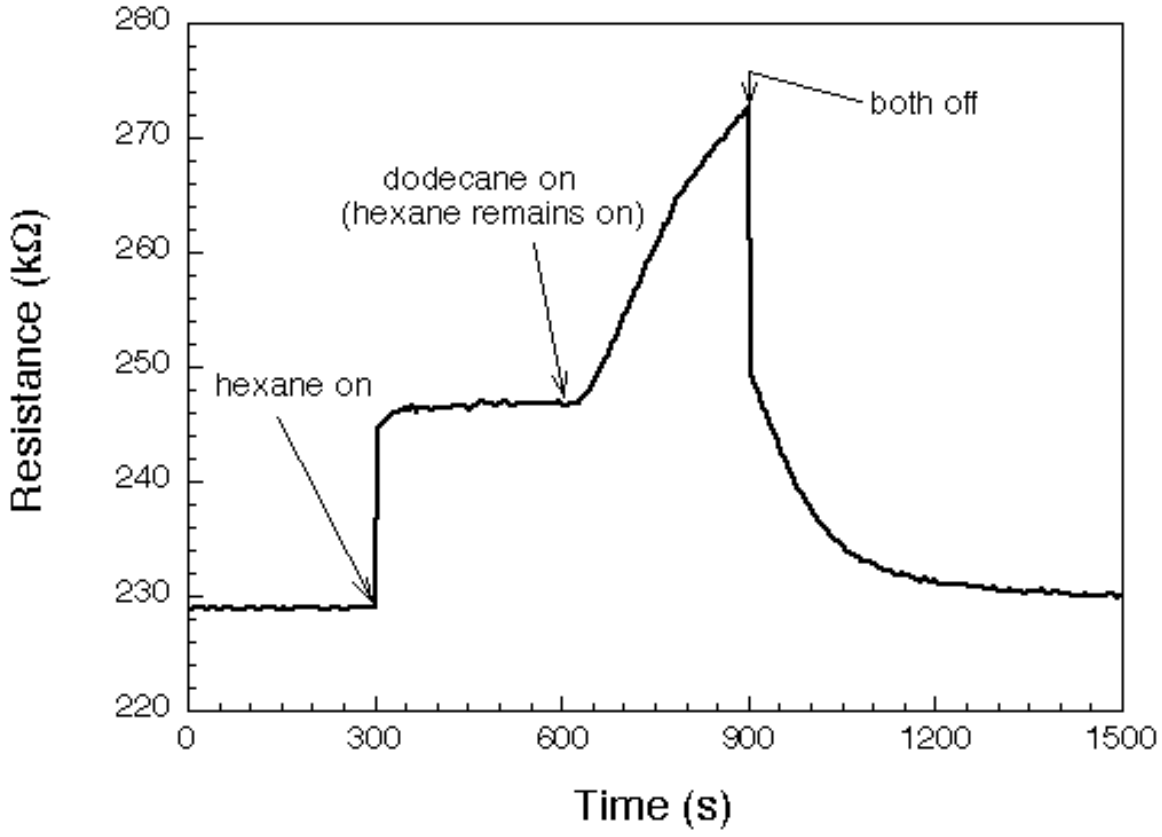

Fig. 7. Normalized relative differential resistance responses, $(\Delta R/R^i) / (\Delta R/R^i)_j$, of a) carbon black-PEVA composite vapor detectors and b) carbon black-PCL detectors to hexane (dashed lines) and dodecane (solid lines) at a constant activity of $P/P^o = 0.10$ in an air background. Data are averages of 5 responses, and the error bars indicate plus and minus one standard deviation values around the mean. Data were obtained from $\Delta R/R^i$ values observed between 240 and 260 s after initiation of exposure to the analyte of interest. For each flow rate, hexane and dodecane were alternately presented to the detectors. This procedure was repeated for each of 5 flow rates, proceeding sequentially from the lowest volumetric flow rate to the highest volumetric flow rate. This 10 exposure protocol was then repeated 4 times, producing 50 total exposures of analyte to the detectors. The detectors were arranged in a linear geometry as depicted in Scheme II, and the analyte flowed from the leftmost detector (corresponding to the detector with the lowest numbered position) towards the rightmost detector. The volumetric flow rate was varied in five values between 6 ml min^{-1} and 100 ml min^{-1}. The data (and associated standard deviations) collected for each flow rate were separately normalized to the mean response value at that flow rate of analyte for the detector in position 1 (j=1) of the array. Normalization constants (volumetric flow rate in ml min^{-1}) for the hexane data of a) are 10.8, (6); 10.5 (14); 10.0 (32); 10.3 (50); 11.1 (100). Normalization constants (volumetric flow rate in ml min^{-1}) for the dodecane data of a) are 26.7, (6); 20.4 (14); 16.8 (32); 16.5 (50); 16.8 (100). Normalization constants (volumetric flow rate in ml min^{-1}) for the hexane data of b) are 45.7, (6); 44.9 (14); 45.0 (32); 46.0 (50); 49.6 (100). Normalization constants (volumetric flow rate in ml min^{-1}) for the dodecane data of b) are 79.5, (6); 67.0 (14); 59.2 (32); 60.5 (50); 64.4 (100).

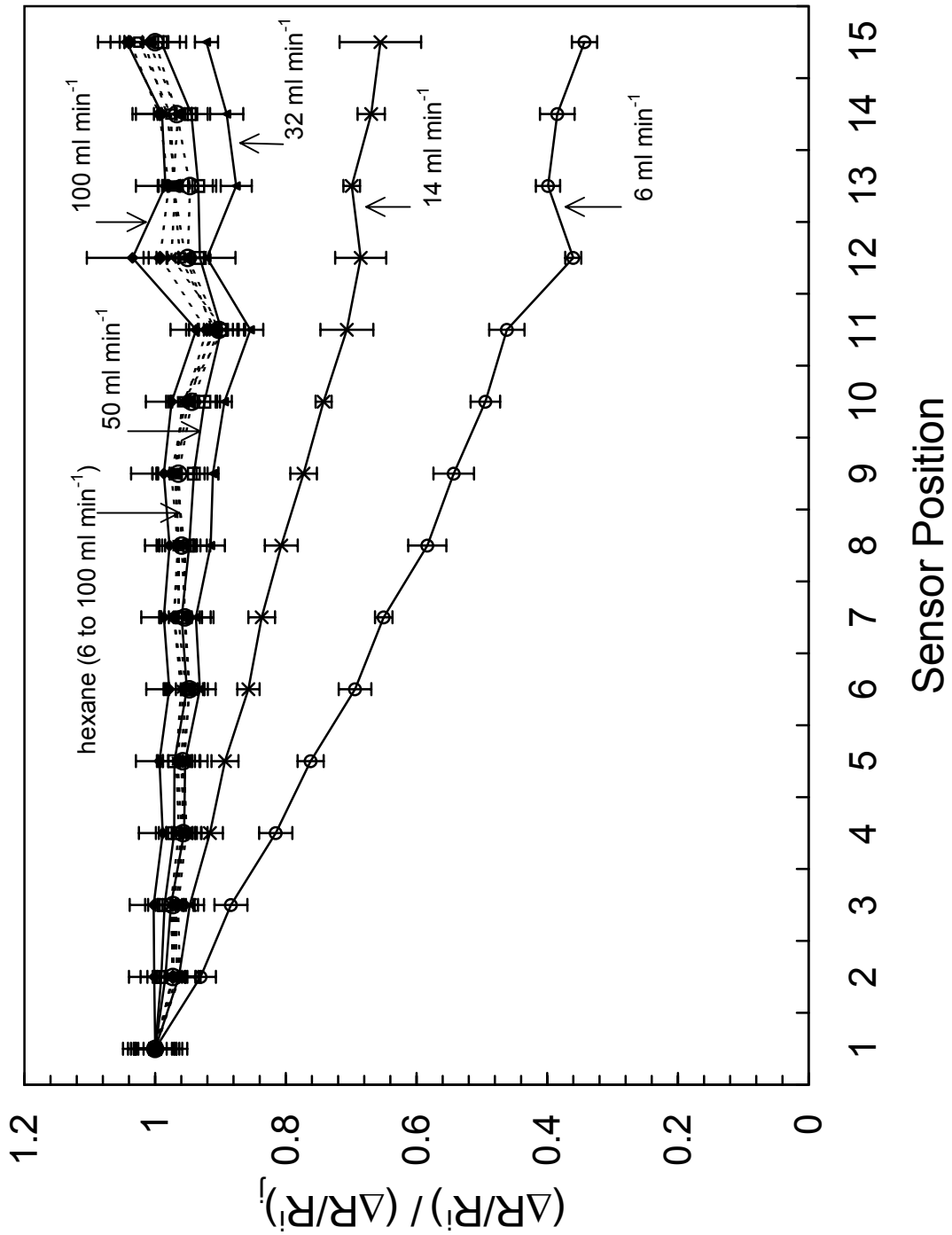
hexane (6 to 100 ml min-1)
50 ml min-1
100 ml min-1
32 ml min-1
14 ml min-1
6 ml min-1
(ΔR/R)i / (ΔR/R)j
Sensor Position
0
0.2
0.4
0.6
0.8
1
1.2
1
2
3
4
5
6
7
8
9
10
11
12
13
14
15

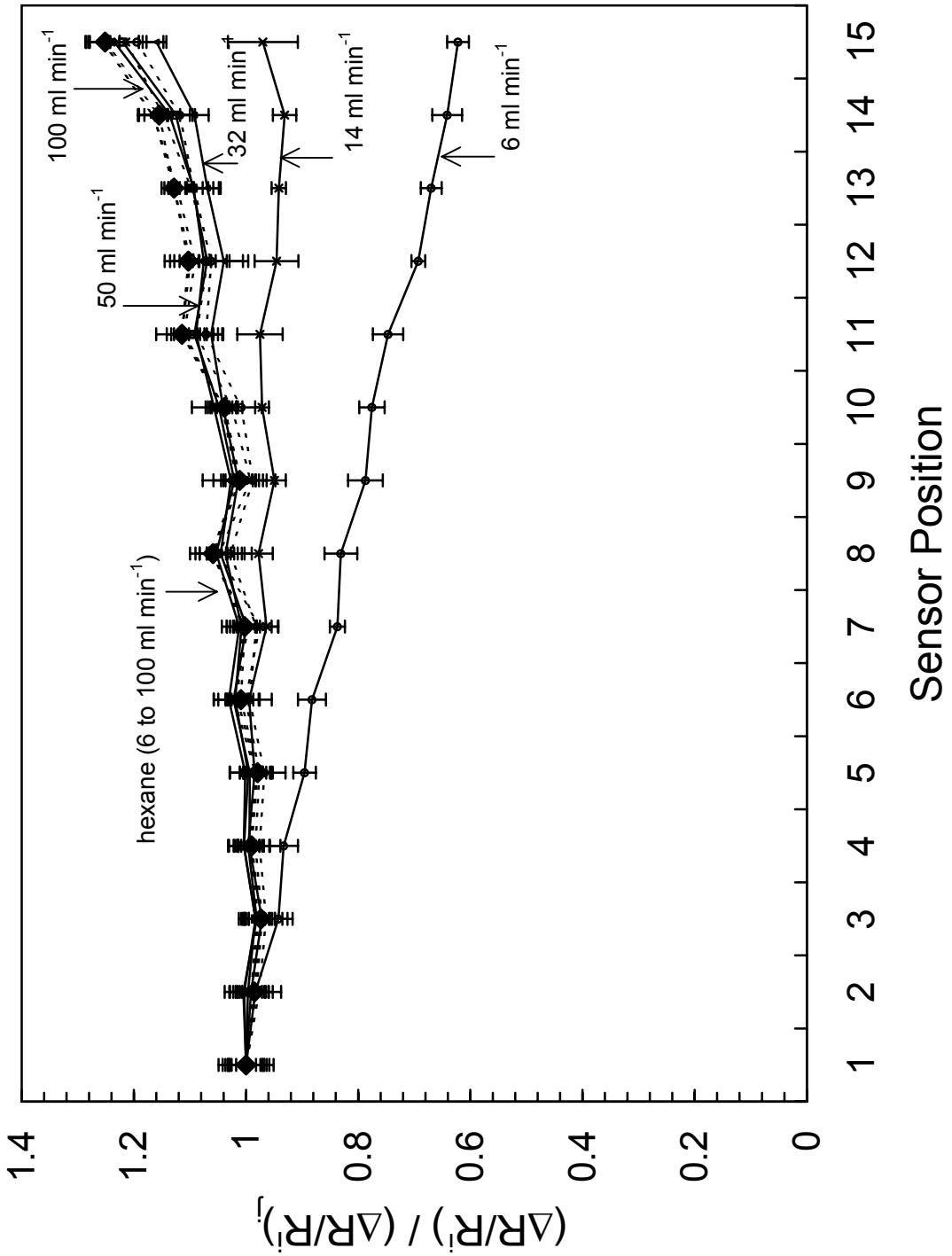
100 ml min-1
50 ml min-1
32 ml min-1
14 ml min-1
6 ml min-1
hexane (6 to 100 ml min-1)
(ΔR/Ri) / (ΔR/Ri)j
Sensor Position
0
0.2
0.4
0.6
0.8
1
1.2
1.4
1
2
3
4
5
6
7
8
9
10
11
12
13
14
15

Fig. 8. Relative differential resistance responses to hexane (diagonal lines) and dodecane (gray) after a) 40 s, and b) 200 s of carbon black composite detectors on the edge and face positions of the substrates arranged in the stacked configuration of Scheme III. Data are averages of 30 $\Delta R/R^i$ responses, representing 10 responses to detectors of the same position on each of the three stack assemblies. The error bars indicate plus and minus one standard deviation value around the mean response value of these 30 detector/analyte combinations. Each analyte was delivered at $P/P^o = 0.050$ in a laboratory air background.

a)

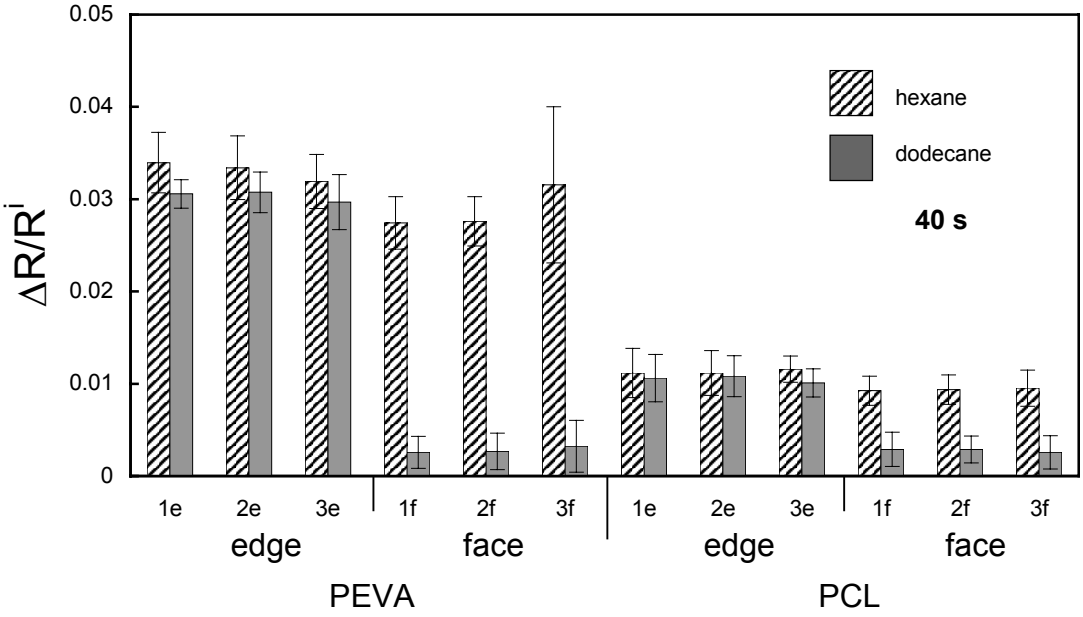
0.05
0.04
0.03
0.02
0.01
0
ΔR/R^i
hexane
dodecane
40 s
1e
2e
3e
1f
2f
3f
edge
face
PEVA
PCL

b)

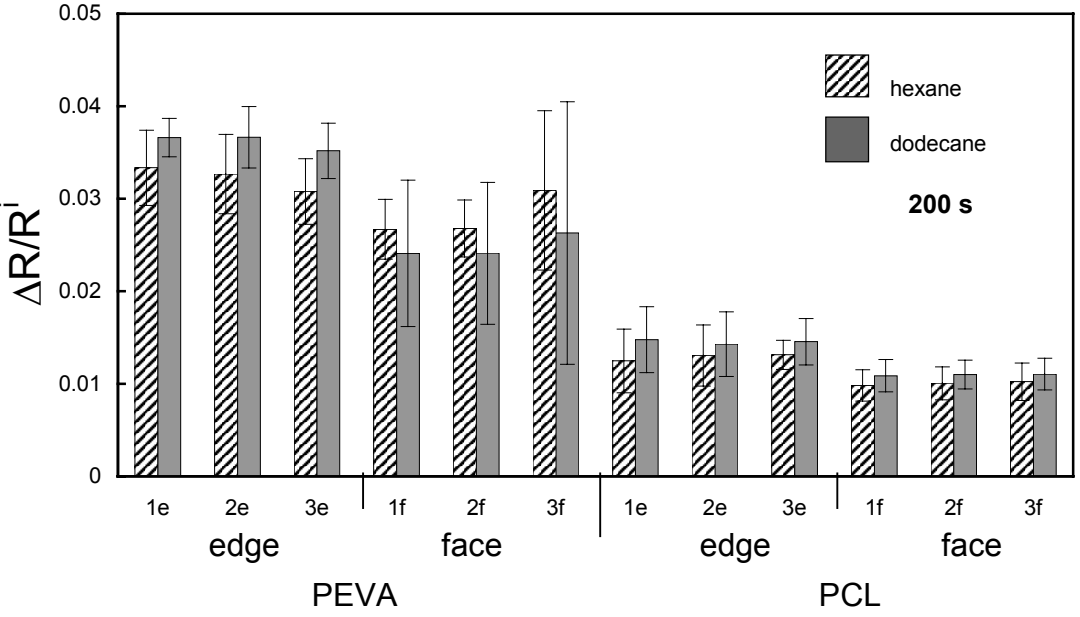
0.05
0.04
0.03
0.02
0.01
0
ΔR/R^i
hexane
dodecane
200 s
1e
2e
3e
1f
2f
3f
edge
face
PEVA
PCL

X. REFERENCES

1. M. C. Lonergan, E. J. Severin, B. J. Doleman, S. A. Beaber, R. H. Grubb, N. S. Lewis, Array-based vapor sensing using chemically sensitive, carbon black-polymer resistors, Chem. Mat. 8 (1996) pp. 2298-2312
2. J. White, J. S. Kauer, T. A. Dickinson, D. R. Walt, Rapid analyte recognition in a device based on optical sensors and the olfactory system, Anal. Chem. 68 (1996) pp. 2191-2202
3. B. J. Doleman, R. D. Sanner, E. J. Severin, R. H. Grubbs, N. S. Lewis, Use of compatible polymer blends to fabricate arrays of carbon black-polymer composite vapor detectors, Anal. Chem. 70 (1998) pp. 2560-2564
4. E. Benes, M. Groschl, W. Burger, M. Schmid, Sensors based on piezoelectric resonators, Sens. Actuator A-Phys. 48 (1995) pp. 1-21
5. J. W. Grate, M. Klusty, Surface acoustic-wave vapor sensors based on resonator devices, Anal. Chem. 63 (1991) pp. 1719-1727
6. S. M. Briglin, C. M. Burl, M. S. Freund, N. S. Lewis, A. Matzger, D. N. Ortiz, P. Tokumaru, Progress in use of carbon black-polymer composite vapor detector arrays for land mine detection, Proc. SPIE-Int. Opt. Eng. 4038 (2000).
7. T. H. Wilmshurst. *Signal Recovery from Noise in Electronic Instrumentation*, Adam Hilger Ltd., Boston, 1985.
8. M. B. Weissman, 1/f noise and other slow, nonexponential kinetics in condensed matter, Rev. Mod. Phys. 60 (1988) pp. 537-571
9. J. R. Larry, R. M. Rosenberg, R. O. Uhler, Thick-film technology: an introduction to the materials, IEEE Transactions on Components Hybrids and Manufacturing Technology 3 (1980) pp. 211-225
10. A. Dziedzic, A. Kolek, 1/f noise in polymer thick-film resistors, J. Phys. D-Appl. Phys. 31 (1998) pp. 2091-2097

11. J. H. Scofield, D. H. Darling, W. W. Webb, Exclusion of temperature-fluctuations as the source of 1/f noise in metal-films, Phys. Rev. B 24 (1981) pp. 7450-7453

12. S. L. Fu, M. S. Liang, T. Shiramatsu, T. S. Wu, Electrical characteristics of polymer thick-film resistors. 1. Experimental results, IEEE Transactions on Components Hybrids and Manufacturing Technology 4 (1981) pp. 283-288

13. K. J. Albert, N. S. Lewis, C. L. Schauer, G. A. Sotzing, S. E. Stitzel, T. P. Vaid, D. R. Walt, Cross-reactive chemical sensor arrays, Chem. Rev. 100 (2000) pp. 2595-2626

14. M. J. Deen, S. Rumyantsev, J. Orchard-Webb, Low frequency noise in heavily doped polysilicon thin film resistors, J. Vac. Sci. Technol. B 16 (1998) pp. 1881-1884

15. E. J. Severin, N. S. Lewis, Relationships among resonant frequency changes on a coated quartz crystal microbalance, thickness changes, and resistance responses of polymer-carbon black composite chemiresistors, Anal. Chem. 72 (2000) pp. 2008-2015

16. A. Peled, R. E. Johanson, Y. Zloof, S. O. Kasap, 1/f noise in bismuth ruthenate based thick-film resistors, IEEE Trans Compon. Packag. Manuf. Technol. Part A 20 (1997) pp. 355-360

17. P. Horowitz, W. Hill. *The Art of Electronics*, Cambridge University Press, New York, 2nd edn., 1989.

18. C. Lu. *Applications of Piezoelectric Quartz Crystal Microbalances*, Elsevier, New York, 1984.

19. D. A. Buttry. *Electroanalytical Chemistry; A Series of Advances*, Vol. 17, Marcel Dekker, New York, 1991.

20. B. J. Doleman, E. J. Severin, N. S. Lewis, Trends in odor intensity for human and electronic noses: relative roles of odorant vapor pressure vs. molecularly specific odorant binding, Proc. Natl. Acad. Sci. U.S.A. 95 (1998) pp. 5442-5447

21. E. J. Severin, B. J. Doleman, N. S. Lewis, An investigation of the concentration dependence and response to analyte mixtures of carbon black/insulating organic polymer composite vapor detectors, Anal. Chem. 72 (2000) pp. 658-668

22. S. J. Patrash, E. T. Zellers, Characterization of polymeric surface-acoustic-wave sensor coatings and semiempirical models of sensor responses to organic vapors, Anal. Chem. 65 (1993) pp. 2055-2066

23. E. T. Zellers, J. Park, T. Hsu, W. A. Groves, Establishing a limit of recognition for a vapor sensor array, Anal. Chem. 70 (1998) pp. 4191-4201

24. M. la Grone, C. Cumming, M. Fisher, D. Reust, R. Taylor, Landmine detection by chemical signature: detection of vapors of nitroaromatic compounds by fluorescence quenching of novel polymer materials, Proc. SPIE-Int. Opt. Eng. 3710 (1999) pp. 409-420

25. V. George, T. F. Jenkins, D. C. Leggett, J. H. Cragin, J. Phelan, J. Oxley, J. Pennington, Progress on determining the vapor signature of a buried land mine, Proc. SPIE-Int. Opt. Eng. 3710 (1999) pp. 258-269

26. N. Sobel, R. M. Khan, A. Saltman, E. V. Sullivan, J. D. E. Gabrieli, Olfaction: the world smells different to each nostril, Nature 402 (1999) pp. 35-35

27. Reprinted with permission from Sens. Actuator B-Chem, 82, S. M. Briglin, M. S. Freund, P. Tokumaru, N. S. Lewis, Exploitation of spatiotemporal information and geometric optimization of signal/noise performance using arrays of carbon black-polymer composite vapor detectors, pp. 54-74, (2002), with permission from Elsevier.

XI. APPENDICES

Appendix A. A dimensioned drawing of the low volume linear chamber used in the Scheme II experiments. Two identical pieces were used to form the chamber around the glass slide substrate.

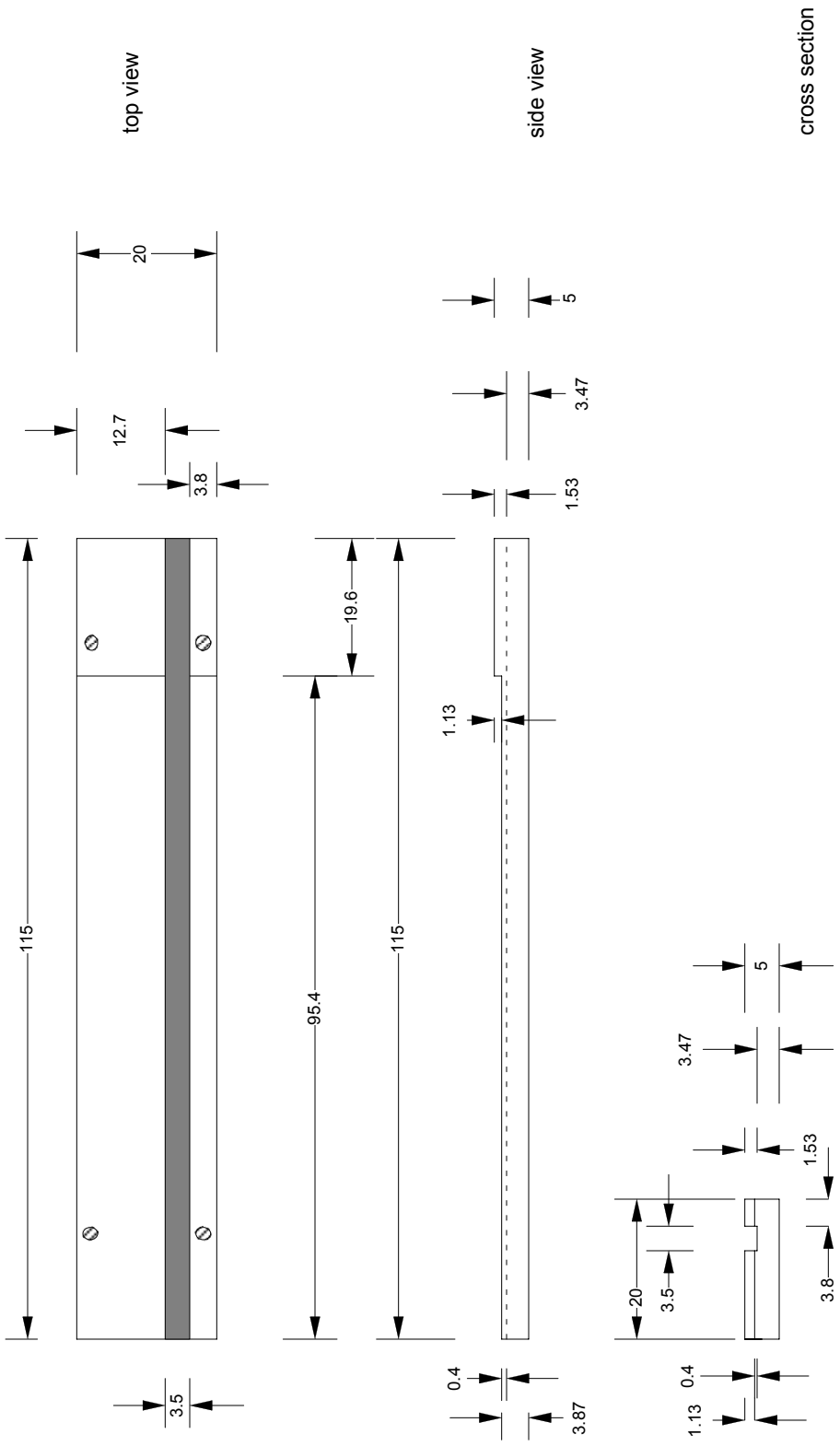
top view
side view
cross section
115
20
12.7
3.8
3.5
95.4
19.6
115
1.13
0.4
3.87
5
3.47
1.53
20
3.5
3.8
0.4
1.13